Open Access

IJCER ONLINE

ISSN Online: 2250–3005

Impact Factor: 1.145

IJCER - International Journal of Computational Engineering Research

Volume 05 – Issue 11, (November 2015)

www.ijceronline.com– Email–ijceronline@gmail.com

Editorial Board

Editor-In-Chief

Editorial Committees

Contents:

ISSN (e): 2250 – 3005 || Volume, 05 || Issue, 11 ||November – 2015 ||
International Journal of Computational Engineering Research (IJCER)

Design And Analysis of a Rocker Arm

Jafar Sharief[1], K.Durga Sushmitha[2]
[1]Mtech student, Nimra College of engineering & technology, Ibrahimpattanam, AP, INDIA,
[2]Guide (Asst.Professor), Nimra College of engineering & technology, Ibrahimpattanam, AP, INDIA.

ABSTRACT
Rocker arms are part of the valve-actuating mechanism. A rocker arm is designed to pivot on a pivot pin or shaft that is secured to a bracket. The bracket is mounted on the cylinder head. One end of a rocker arm is in contact with the top of the valve stem, and the other end is actuated by the camshaft. In installations where the camshaft is located below the cylinder head, the rocker arms are actuated by pushrods. The lifters have rollers which are forced by the valve springs to follow the profiles of the cams. Failure of rocker arm is a measure concern as it is one of the important components of push rod IC engines.Present work finds the various stresses under extreme load condition. For this we are modeling the arm using design software and the stressed regions are found out usingAnsys software. Here in this thesis we are observing that by changing different materials how the stresses are varying in the rocker arm under extreme load condition. And after comparing results we are proposing best suitable material for the rocker arm under extreme load conditions.
Key words:*Ansys, camshaft, pro-e and rocker arm*

I. INTRODUCTION

1.1 Introduction and working of Rocker arm

Rocker arm is an important part of the valve train in fuel injection system providing not only the means of actuating the valves through a fulcrum utilizing the lifter and the push rod but also provide a means of multiplying the lift ratio. Cam shaft design has advanced in leaps and bounds over last three decades but overhead valve engines with centrally located camshafts still use lifters and push rod and rocker arms as a means of opening and closing the intake and exhaust valves in fuel injection pumps. Advancement in materials used in construction of rocker arm for reducing the noise, weight and higher strength for efficient operation is going on throughout the globe since long. The usual materials used for such purpose are Steel, Aluminum, and Forged steel to Stainless steel, alloys and composites. The success to investigate the possibility creating a light weight rocker arm that could provide a friction reducing fulcrum using needle bearings and a roller tip for reduced friction between the rocker and the valve stem but still be less expensive than steel lies in the development of composite rocker arms. Lighter mass at the valve is also allowed for increased speed while strength of the material caters to durability. The rocker arm usually operates at 40-500 C and the maximum pressure is exerted by the gas. Therefore in this investigation it has been thought proper to analyze a composite rocker arm of high density polyethylene (HDPE) reinforced with short S-glass fibers of 10% volume fraction. Finite element analysis may be carried out to determine the stresses and make a comparison between steel and composite to predict the failure modes.

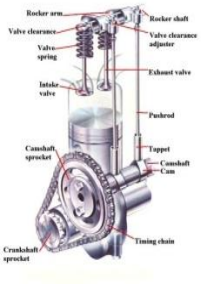

Fig.1 Rocker armFig.2 Position of Rocker arm

II. MODELLING BY USING PRO-E

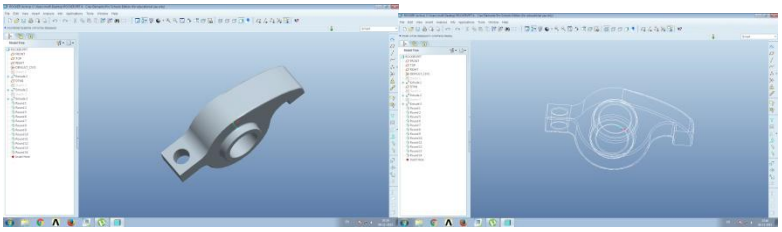

Fig.3 Solid model Fig .4 Wire frame model

III. ANALYSIS BY ANSYS

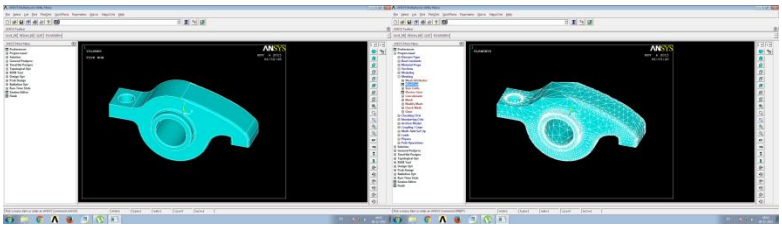

Fig.5 Imported model Fig.6 Meshed model

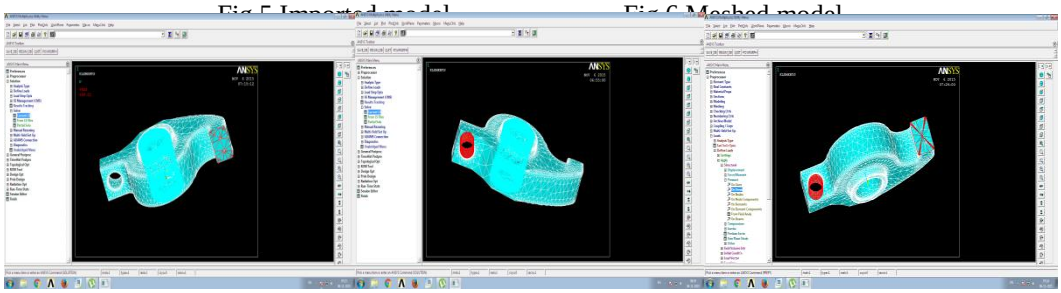

Fig.7 Load distribution at endFig.8 Load distribution at pin Fig.9 Load distribution at pin and end

IV. RESULTS AND DISCUSSION

4.1 Structural analysis

4.1.1 Load distribution at end

a) Alloy steel -1

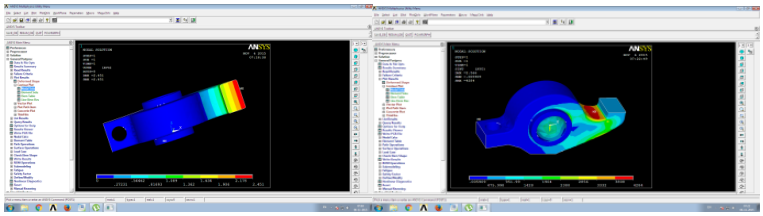

Fig.10 Total deformation Fig.11 Stress intensity

b) Alloy steel -2

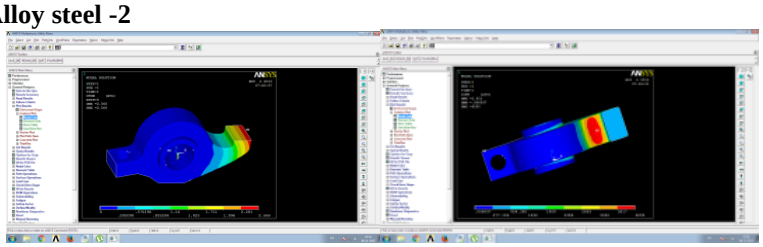

Fig.12 Total deformation Fig.13 Stress intensity

c) Composite material

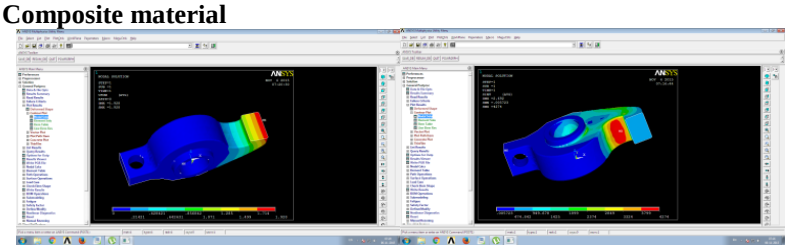

Fig.14 Total deformation Fig.15 Stress intensity

d) Steel

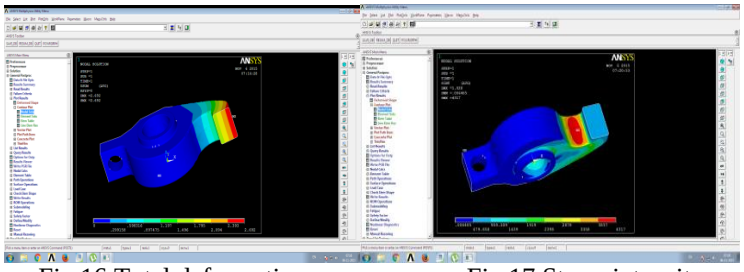

Fig.16 Total deformation Fig.17 Stress intensity

4.1.2 Load distribution at pin

a) Alloy steel -1

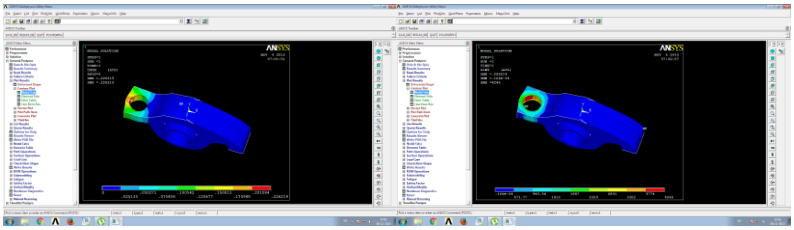

Fig.18 Total deformation Fig.19 Stress intensity

b) Alloy steel -2

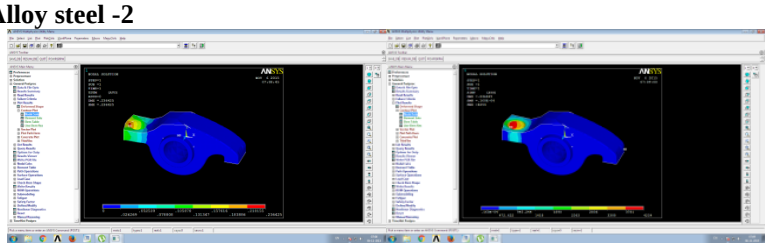

Fig.20 Total deformation Fig.21 Stress intensity

c) Composite material

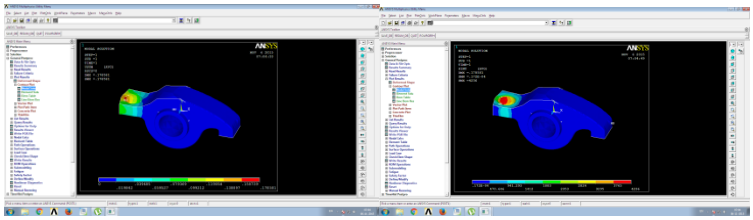

Fig.22 Total deformation Fig.23 Stress intensity

d) Steel

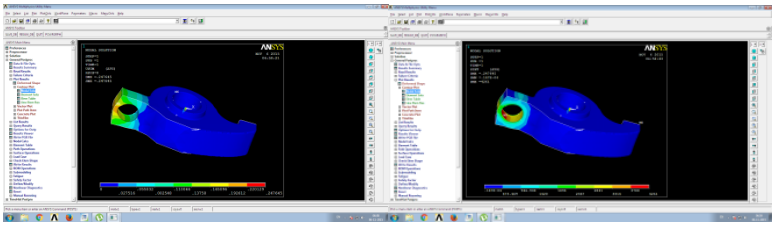

Fig.24 Total deformation Fig.25 Stress intensity

4.1.3 Load distribution atboth pin and end

a) Alloy steel -1

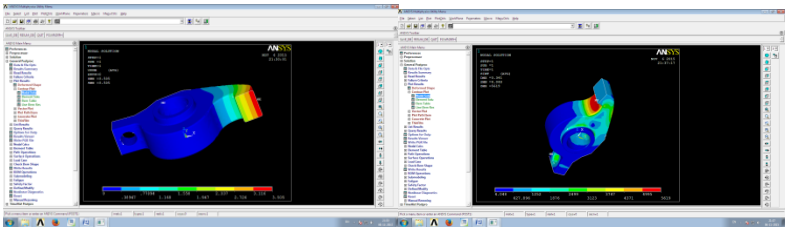

Fig.26 Total deformation Fig.27 Stress intensity

b) Alloy steel -2

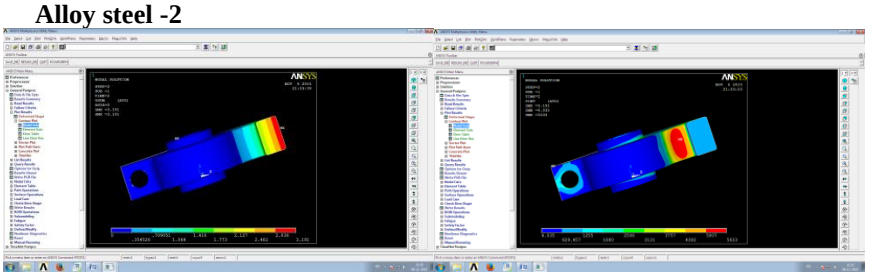

Fig.28 Total deformation Fig.29 Stress intensity

c) Composite material

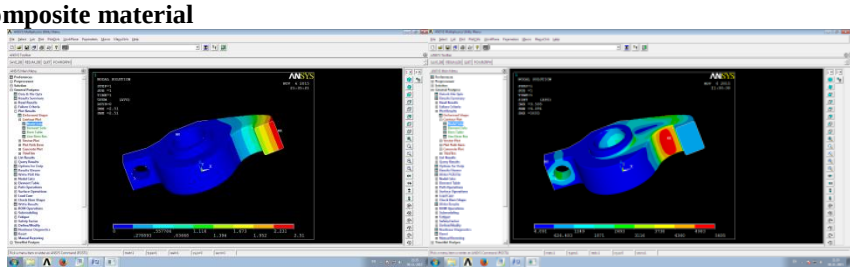

Fig.30 Total deformation Fig.31 Stress intensity

d) Steel

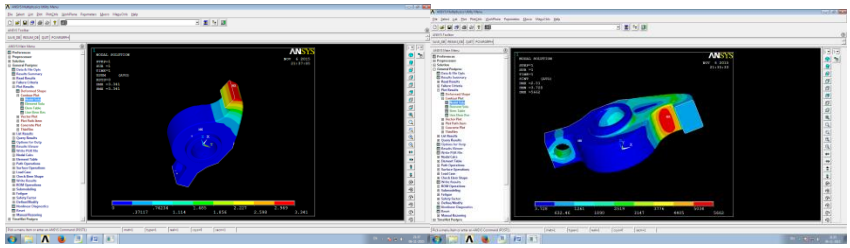

Fig.32 Total deformation Fig.33 Stress intensity

4.2 Results and comparisons

4.2.1 Load at pin

SNO	MATERIAL	TOTAL DEFORMATION	STRESS INTENSITY
1	Alloy steel-1	.2262	4246
2	Alloy steel -2	.2364	4254
3	Composite	.1785	4236
4	Steel	.2476	4261

Table no.1 Load deformation at pin

4.2.2 Load at end

SNO	MATERIAL	TOTAL DEFORMATION	STRESS INTENSITY
1	Alloy steel-1	2.451	4284
2	Alloy steel-2	2.566	4294
3	Composite	1.928	4274
4	Steel	2.692	4317

Table no.2 Load deformation at end

4.2.3 Load at both pin and end

SNO	MATERIAL	TOTAL DEFORMATION	STRESS INTENSITY
1	Alloy steel-1	3.505	5619
2	Alloy steel -2	3.191	5633
3	Composite	2.51	5605
4	Steel	3.341	5662

Table no.3 Load deformation at pin and end

V. CONCLUSION

The modeling of the rocker arm is done by using pro-e and the analysis is performed by Ansys. The project consists of structural analysis of rocker arm which is done to find the strength of the model. To find the strength of the model in structural analysis we are taken 4 different materials and taken 3 load points on the model. We did analysis on the model by applying loads at pin and end side by varying different 4 materials.By the results we observed that the stress values of steel and alloy steel materials are nearer to each other and also for the total deformation the values of the steel and alloy steel got nearly same values. But only composite material got the better values in stress intensity and total deformation when compared to other materials.So by the investigation we conclude that by using composite material the stress values are reduced by that the life time of the rocker arm increases.

Future scope

1. By changing the model design and reducing the thickness we may get better values.
2. And also by using advanced smart materials we can increase the performance of the model.

REFERENCES

[1] Z.W. Yu, X.L. Xu "Failure analysis of diesel engine rocker arms" Engineering Failure Analysis, Volume 13, Issue 4, June 2006, Pages 598-605

[2] Chin-Sung Chung, Ho-Kyung Kim "Safety evaluation of the rocker arm of a diesel engine" Materials & Design, Volume 31, Issue 2, February 2010, Pages 940-945`

[3] Dong-Woo Lee, Soo-Jin Lee, Seok-Swoo Cho , Won-Sik Joo "Failure of rocker arm shaft for 4-cylinder SOHC engine"

[4] Dong Woo Lee, Seok Swoo Cho and Won Sik Joo "An estimation of failure stress condition in rocker arm shaft through FEA and microscopic fractography"

[5] Giovanni Scire Mammano and Eugenio Dragoni (2013), "Design and Testing of an Enhanced Shape Memory Actuator Elastically Compensated by a Bistable Rocker Arm", *Structures Journal ofIntelligent Material Systems andStructures*.

[6] Hendriksma N, Kunz T and Greene C (2007), "Design and Development of a 2-Step Rocker Arm", SAE International, USA.

[7] Satpathy, Sukanya, Jose, Jobin, Nag, Ahin and Nando, G.B.," Short Glass Fiber Filled Waste Plastic (PE) Composites- Studies on Thermal and Mechanical Properties, "Progress in Rubber, Plastics and Recycling Technology, Vol.24, No.3, pp.199-218, 2008.

[8] Chung, Chin-Sung and Kim Ho-Kyung, "Safety Evaluation of the Rocker Arm of a Diesel Engine," Materials and Design, Vol.31 (2), pp.940-945, 2010.

[9] Kun Cheng, "Finite element analysis of Rocker Arm of Vertical Roller Mill on ANSYS work Bench "Advanced Materials Research, Vol.230-232, pp.824-828, 2011.

[10] Yang, Changxing., Li, Guan, Qi, Rongrong and Huang, Mark," Glass Fibre/Wood Flour Modified High Density Polyethylene Composites," Jou. of Applied Polymer Science, Vol.123, pp.2084-2089, 2012.

ISSN (e): 2250 – 3005 || Volume, 05 || Issue, 11 ||November – 2015 ||
International Journal of Computational Engineering Research (IJCER)

Stress Analysis of a Centrifugal Supercharger Impeller Blade

Mohammed irafanuddin[1], K. Durga Sushmitha[2]
[1]Mtech student, Nimra College of engineering & technology, Ibrahimpattanam, AP, INDIA,
[2]Guide (Asst.Professor), Nimra College of engineering & technology, Ibrahimpattanam, AP, INDIA.

Abstract
A supercharger is an air compressor that increases the pressure or density of air supplied to an internal combustion engine. This gives each intake cycle of the engine more oxygen, letting it burn more fuel and do more work, thus increasing power. Power for the supercharger can be provided mechanically by means of a belt, gear, shaft, or chain connected to the engine's crankshaft. Superchargers are a type of forced induction system. They compress the air flowing into the engine. The advantage of compressing the air is that it lets the engine squeeze more air into a cylinder, and more air means that more fuel can be added. Therefore, you get more power from each explosion in each cylinder. Here in this project we are designing the compressor wheel by using Pro-E and doing analysis by using FEA package.
An attempt has been made to investigate the effect of pressure and induced stresses on the blade. By identifying the true design feature, the extended service life and long term stability is assured. A structural analysis has been carried out to investigate the stresses, strains and displacements of the blade. An attempt is also made to suggest the best material for an blade of a turbocharger by comparing the results obtained for different materials. Based on the results best material is recommended for the blade of a turbocharger.
Key words: *Air compressor, Ansys, FEA package and supercharger*

I. INTRODUCTION

A supercharger is an air compressor that increases the pressure or density of air supplied to an internal combustion engine. This gives each intake cycle of the engine more oxygen, letting it burn more fuel and do more work, thus increasing power. Turbocharger components are classified as turbine housing (volute), turbine (radial and axial flow type),compressor, compressor wheel (blade), diffuser, bearing system ,bearing housing , control system ,waste gates, inter cooler.

The way to add power is to make a normal-sized engine more efficient. You can accomplish this by forcing more air into the combustion chamber. More air means more fuel can be added, and more fuel means a bigger explosion and greater horsepower. Adding a **supercharger** is a great way to achieve forced air induction. In this article, we'll explain what superchargers are, how they work and how they compare to turbochargers. A supercharger is any device that pressurizes the air intake to above atmospheric pressure. Both superchargers and turbochargers do this. In fact, the term "turbocharger" is a shortened version of "turbo-supercharger," its official name. The difference between the two devices is their source of energy. Turbochargers are powered by the mass-flow of exhaust gases driving a turbine. Superchargers are powered mechanically by belt- or chain-drive from the engine's crankshaft.

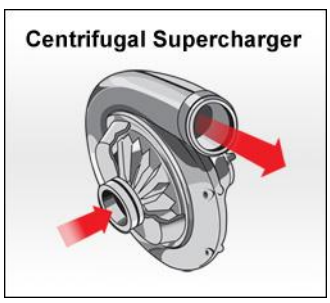

Fig. no 1 Dynamic compressor

The Centrifugal supercharger is used in many applications including, but not limited to, automotive, truck, marine, aircraft, motorcycles and UTV's. Of these applications, they are most commonly utilized for increasing horsepower in street vehicles and race applications. While the first practical centrifugal compressor was designed in 1899, centrifugal superchargers evolved during World War II with their use in aircraft, where they were frequently paired with their exhaust driven counterpart, the turbo supercharger. This term refers to the fact that turbochargers are a specific type of centrifugal supercharger, one that is driven by a turbine.

- Automotive Superchargers
- Aircraft Superchargers

Centrifugal superchargers have become popular in the aftermarket as a bolt-on addition to improve performance. By design, centrifugal superchargers allow for easy integration of air-to-air or air-to-water inter cooling.

Superchargers in aircraft play an important role by providing additional air pressure at higher altitudes. Because air pressure decreases at high altitudes, air compression is necessary in order to keep the airplane's engine running at maximum efficiency.

II. MODELLING OF COMPRESSOR BLADE

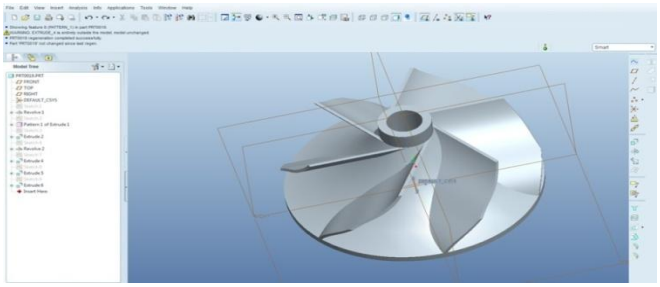

Fig. no 2 Solid model of compressor

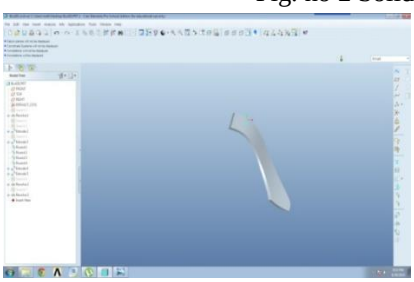

Fig. no 3 actual blade model with thickness = t

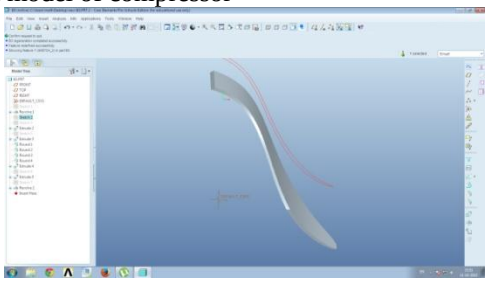

Fig. no 4 modified blade model with thickness = t – 0.5 mm

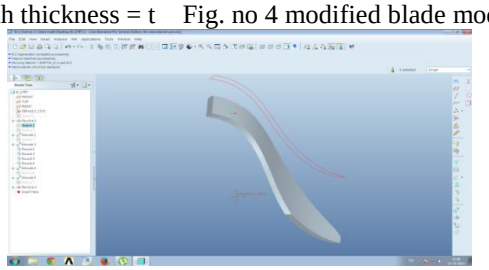

Fig. no 5 modified blade model with thickness = t + 0.5mm

III. ANALYSIS OF COMPRESSOR BLADE

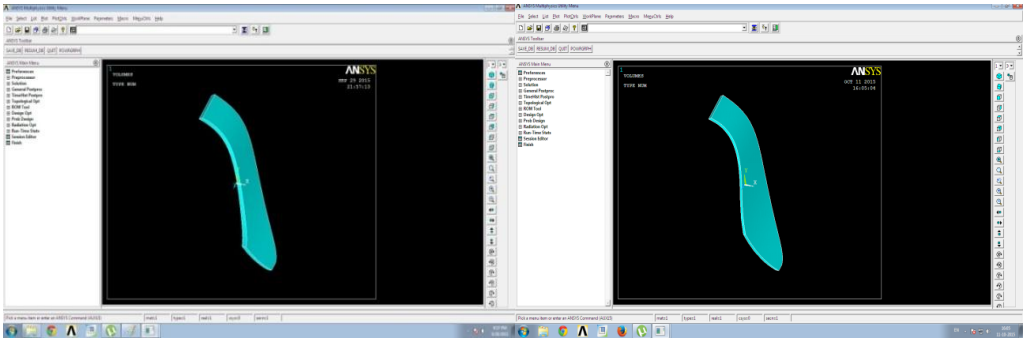

Fig. no 6 Imported model of actual blade with thickness = t

Fig. no 7 Imported model of modified blade with thickness = t – 0. 5 mm

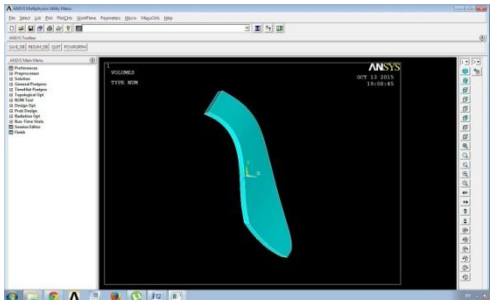

Fig. no 8 Imported model of modified blade with thickness = t + 0. 5 mm

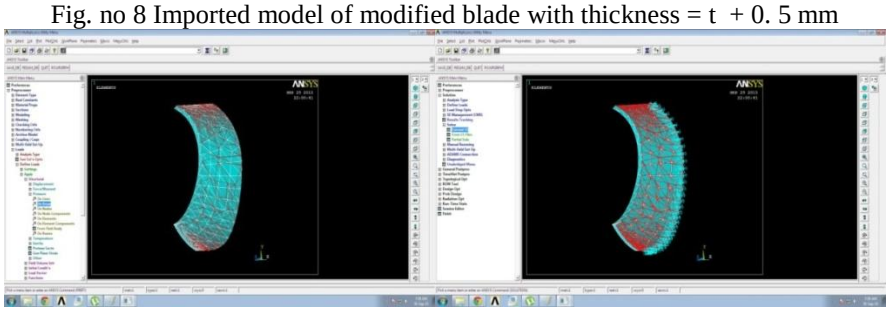

Fig. no 9 Applying load on surface of blade

Fig. no 10 Load distribution on blade

IV. RESULTS AND DISCUSSION

Structural analysis

4.1 ACTUAL MODEL WITH THICKNESS = T

a) ALLOY 706

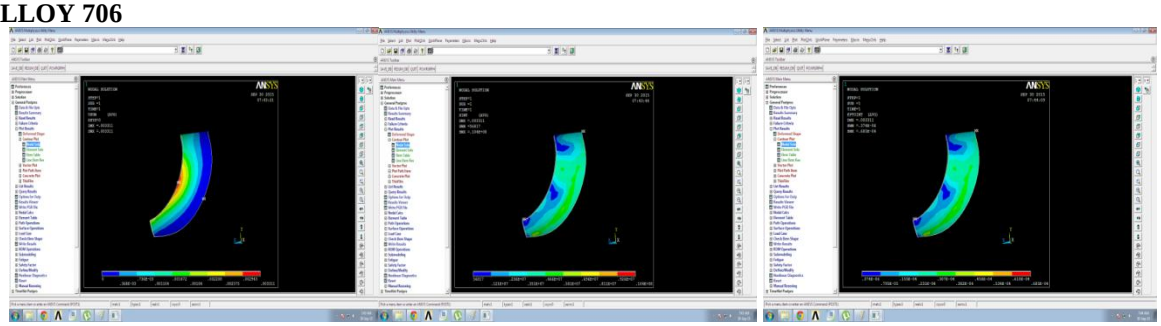

Fig. no 11 Total deformation

Fig. no 12 Stress intensity

Fig. no 13 Strain intensity

b) Composite alloy

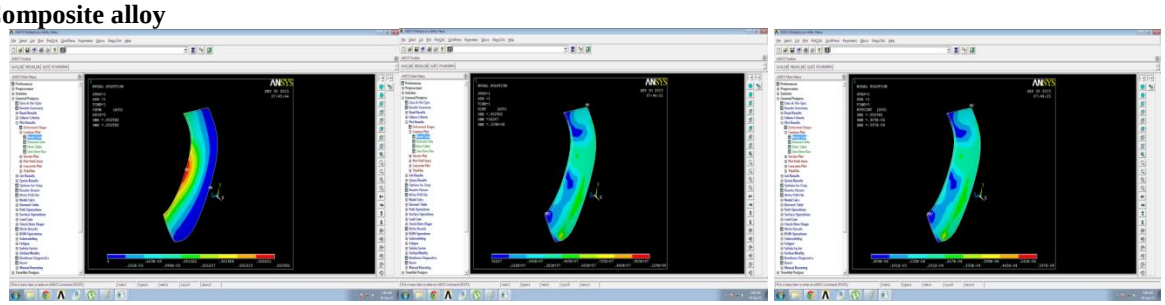

Fig. no 14 Total deformation

Fig. no 15 Stress intensity

Fig. no 16 Strain intensity

c) Steel

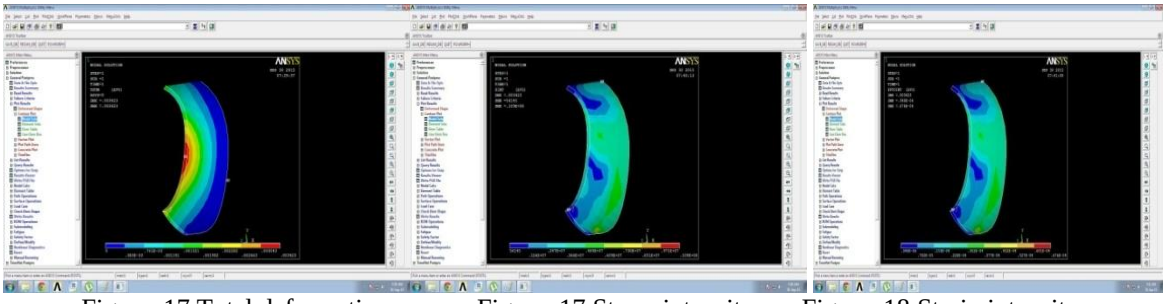

Fig. no 17 Total deformation

Fig. no 17 Stress intensity

Fig. no 18 Strain intensity

4.2 MODIFIED MODEL WITH THICKNESS = T - 0.5 mm

a. Composite alloy

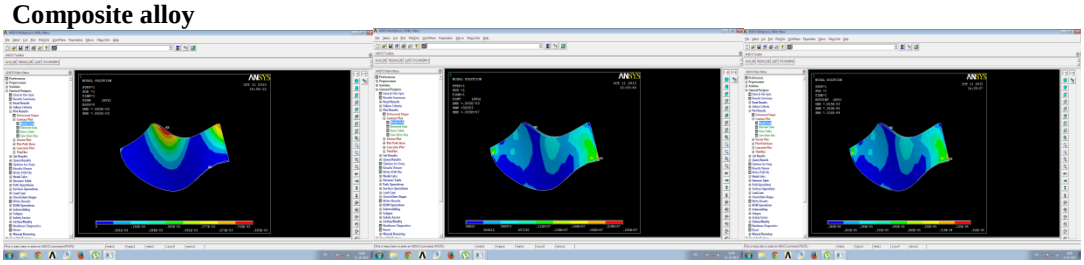

Fig. no 19 Total deformation Fig. no 20 Stress intensity Fig. no 21 Strain intensity

b. Alloy 706

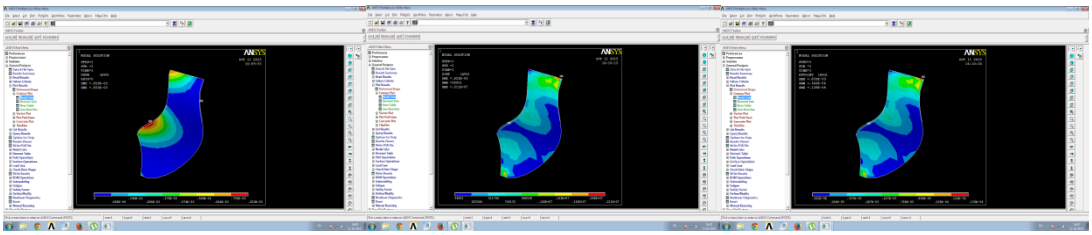

Fig. no 22 Total deformation Fig. no23 Stress intensity Fig. no24 Strain intensity

d) **Steel**

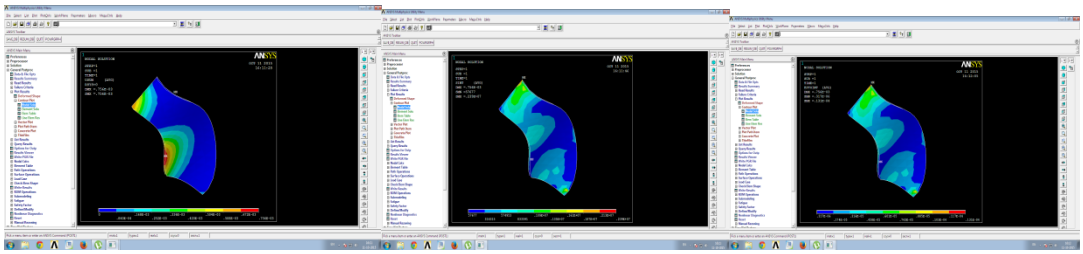

Fig. no25 Total deformation Fig. no 26 Stress intensity Fig. no 27 Strain intensity

4.3 MODIFIED MODEL WITH THICKNESS = T + 0.5 mm

a. Composite alloy

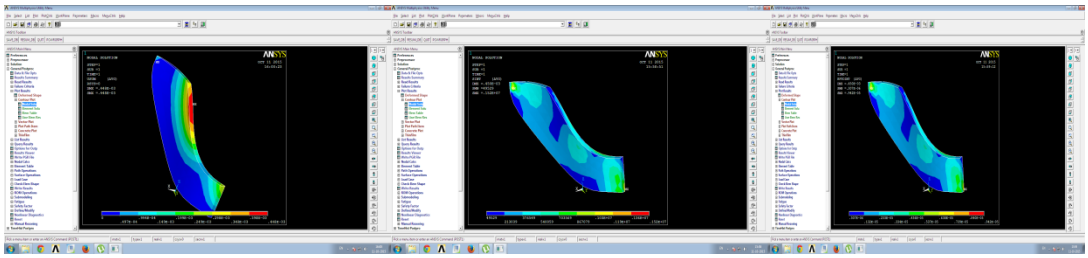

Fig. no 28 Total deformation Fig. no 29 Stress intensity Fig. no 30 Strain intensity

b. Alloy 706

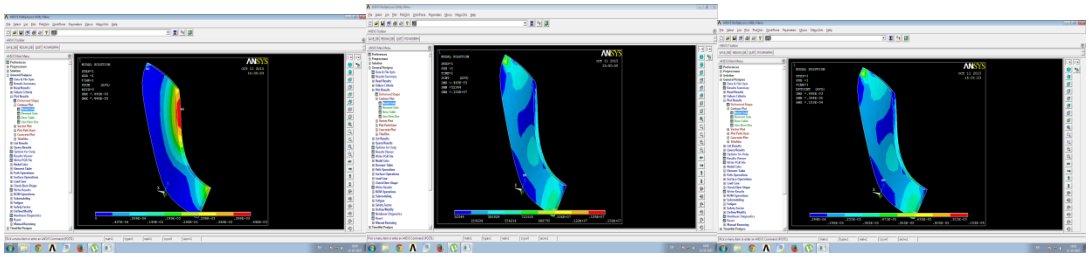

Fig. no 31 Total deformation Fig. no 32 Stress intensity Fig. no 33 Strain intensity

c. Steel

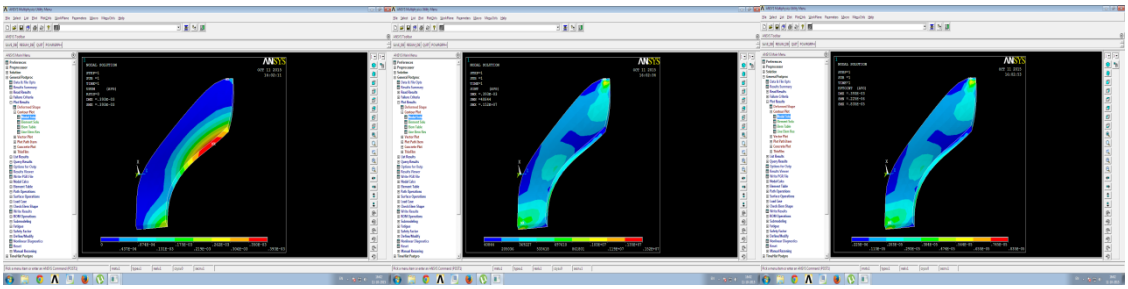

Fig. no 34 Total deformation Fig. no 35 Stress intensity Fig. no 36 Strain intensity

5.4 Comparison of results

SNO	MATERIAL	TOTAL DEFORMATION	STRAIN INTENSITY
1	Alloy 706	.003311	.685E-04
2	Composite alloy	.002982	.597E-04
3	Steel	.003423	.676E-04

Table no 1. Comparison of actual blade model with thickness = t

SNO	MATERIAL	TOTAL DEFORMATION	STRAIN INTENSITY
1	Alloy 706	.865 E-03	.245E+07
2	Composite alloy	.756E-03	.211E+07
3	Steel	.853E-03	.239E+07

Table no 2. Comparison of modified blade model with thickness = t – 0.5 mm

SNO	MATERIAL	TOTAL DEFORMATION	STRAIN INTENSITY
1	Alloy 706	.450 E-03	.152E+07
2	Composite alloy	.393E-03	.152E+07
3	Steel	.448E-03	.156E+07

Table no 3. Comparison of modified blade model with thickness = t + 0.5

V. Conclusion

The analysis of supercharger compressor blade done to investigate the effect of pressure and induced stresses on the blade. A structural analysis has been carried out to observe the stresses, strains and displacements of the blade.

- The analysis is performed by two alloy materials with actual steel material.
- After the analysis the comparison is made.
- By those values we observed that the stress and deformation values of the actual material steel and alloy 706 are nearly same.
- And we conclude that the stress values of the composite alloy are better than the other two materials.
- The deformation is also less for the composite alloy when compared to other two materials.

So we suggest composite alloy material to the companies to increase the performance of the super charger compressor blade.

And also by observing the results of the actual blade thickness with the increasing and decreasing thick about 0.5mm the results are slightly changed.

By this we conclude that with the good composite material we may reduce the size (thickness) of the model also.

REFERENCES

[1] Dipl.-Ing. Jonas Belz and Dipl.-Ing. Ralph-Peter Müller "rapid Design and Flow Simulations for Turbocharger Components" EASC ANSYS Conference 2009 RAPID, CFDnetwork® Engineering, CFturbo® Software & Engineering GmbH.
[2] MeinhardSchobeiri. Turbo machinery Flow Physics and Dynamic Performance. Springer, 2005.
[3] Kirk, R. G., 1980, "Stability and Damped Critical Speeds: How to Calculate and Interpret the Results,"
[4] Compressed Air and Gas Institute Technical Digest, 12(2), pp. 1-14.
[5] Alsaeed, A. A., 2005, "Dynamic Stability Evaluation of an Automotive Turbocharger Rotor- Bearing System," M.S. Thesis, Virginia Tech Libraries, Blacksburg, VA.
[6] Encyclopedia
[7] Wickypedia
[8] Machine design text book by RS kurmi
[9] Material Handbook of High Performance Alloys, Special Metals Corp., (2001) Mikio Oi, Mariko Suzuki, Natsuko Matsuura "Structural Analysis and Shape Optimization in Turbocharger Development" published in Ishikawajima-Harima Heavy Industries Co., Ltd.
[10] V Rammurti (iitm),D.A Subramani (TEL), Dhridhara (TEL) "Free vibration analysis of turbocharger centrifugal compressor blade" published in mech march .theory vol 30,No 4, pp 619-628,1995 Elsevier science Ltd

ISSN (e): 2250 – 3005 || Volume, 05 || Issue, 11 ||November – 2015 ||
International Journal of Computational Engineering Research (IJCER)

Engendering sustainable socio-spatial environment for tourism activities in the south eastern nigeria: the place of environmental planning and management process.

Edmund A. Iyi (PhD) [1], Celestine, O. Aniagolu (PhD) [2] and Benneth C. Ugwuanyi[3]

[1 & 3:] Department of Urban and Regional Planning, Enugu State University of Science and Technology (ESUT)
[2:] Department of Estate Management, Enugu State University of Science and Technology (ESUT)

Abstract

The South Eastern part of Nigeria was a single state of the twelve states of Nigeria before 1976 – East Central State. Presently, the area is made up of five states. This Paper presents a study carried out to assess the possibility of knitting the once-one-state and presently five states, together to form a tourist destination worthy of international importance. Although the unprecedented dearth of infrastructural development in the zone continues to be a subject of discussion, little attention has been given to investigate the place of synergized intervention. Descriptive analysis was employed, in which the tourism potentials in the zone that are of national recognition were itemized. Data were collected on available amenities, resident population and accessibility of such potentials. Existing literature on various Environmental Management Systems were explored to elicit a system that is capable of affording a sustainable environment for tourism matters in the zone. The study revealed that the zone exhibits similar socio-economic and physical characteristics that are replete with potentials for improvement for optimum tourism utility in the entire zone. Several measures were advanced in the study to achieve this, chief of which is the adoption of the Environmental Planning and Management (EPM) process.

Key words: *Tourism destination, national significance, tourism potentials, EPM-process.*

I. Introduction

Tourism as an industry did not assume much significance in Nigeria until the end of the Nigeria civil war in 1970. This was when tourists from different parts of the world trooped into the country to witness the effects of the war. Only very few tourist centres of international standards existed before this period. The ones existed consisted of night clubs that provided relaxation avenues for foreigners. Places of this sort were limited to places like Lagos, Calabar, Port-Harcourt, Warri and a few other hinterland towns (Iyi and Ugwu, 2009).

Studies so far on tourism in Nigeria have provided useful insight as to its contributions to development. However, focus of such studies has remained largely at national level. A pertinent question is whether tourism has potentials for revenue mobilization at sub-national levels.

The aim of this paper was to assess the possibility of inducing a unit tourism environment at a sub-level of the national environment. The study area was the South-East geopolitical zone of Nigeria. That was finding a way to knit the five states that make up the zone together, to form a tourist destination that will be worthy of international importance. Descriptive analysis was employed, in which the tourism potentials in the South-East that are of national recognition were itemized. Data were collected on available tourism potentials of national significance and accessibility of such potentials. Existing related literature on various environmental management systems were explored to elicit a system that would afford a sustainable environment for tourism matters in the zone.

II. Literature Review.

The place of tourism industry in national development has gained significant literature. Richardson (2010) argued that tourism sector is the main source of foreign exchange earnings for one-third of developing countries and among the top three sources of export earnings for almost half of all Least Developed Countries (LDCs). Also, according to the World Travel and Tourism Council (WTTC, 2015), there is evidence to support the claim, that tourism has had significant effects on the growth and development of other sectors of the economy of such cities as Hong-Kong, Sydney, London, Tokyo, Paris, Los Angeles, New York, Buenos, Toronto, Madrid, Berlin, Beijing, Rome and Dubai.

In the area of job creation, tourism has been lauded as a major employer of labour in the recent time. The sector has created large number of direct and indirect jobs. Direct jobs include such job in hotels, airlines, restaurants, transportation, and leisure industry. WTTC (2012) also claimed that tourism contributes to general growth in the world's Gross Domestic Product (GDP). The GDP increased from 2.8 percent in 2011 to 3 percent in 2012 due to contribution from travel and tourism.

The significance of tourism as an industry in any economy therefore, cannot be overemphasized. Such significance can apply to any geographical unit, whether a town, a region or a country. Some of the impacts occur only for countries as a result of international travel which finds expression in the balance of payments of individual countries. A system of environmental management has, therefore, to be deduced to extend the experienced significances at national level to other sub-national levels.

The United Nations centre for Human Settlements (UNCHS) and the United Nations Environmental Programme (UNEP) came up with the Environmental Planning and Management (EPM) process in 1987. The process is a continuing and dynamically evolving process whose purpose is to make development progressively more responsive to environmental considerations (UNCHS/UNEP, 1987, Bloxom, 1986, and Wahab, 1998). The process is a participatory, interactive and collaborative approach to planning and management of the environment. Characteristically, it is a network of concerned stakeholders that work together to tackle man-environment relationship issues. In this regard, there is active participation of stakeholders drawn from the public and private sectors, formal and informal (Iyi and Ugwu, 2009).

The EPM process has the following attributes (Wahab, 1998):-

i. Involvement of all that are affected by an identified environmental issue.
ii. Environmental issues are prioritized and dealt with systemically.
iii. It is a bottom-up approach.
iv. Action plans are usually formulated to guide transformation of strategies into practice.
v. Institutionalization of the process which makes it to get the attention of the public institutions.

III. The Study Area

The study area, South-East geo-political zone, is one of the six geo-political zones into which Nigeria is divided. The zone comprises Anambra, Abia, Ebonyi, Enugu and Imo states. It is bounded in the East, South and West by South-West geo-political zone and in the North by the North-central geo-political zone (see Figure 1).

The zone is situated in the lowland forest region of the country. It is located between latitude 5-7 degrees north and 6-8 degrees east. It has a land mass of about 27,000 square kilometers. It is predominantly of the Igbo speaking tribe of Nigeria.

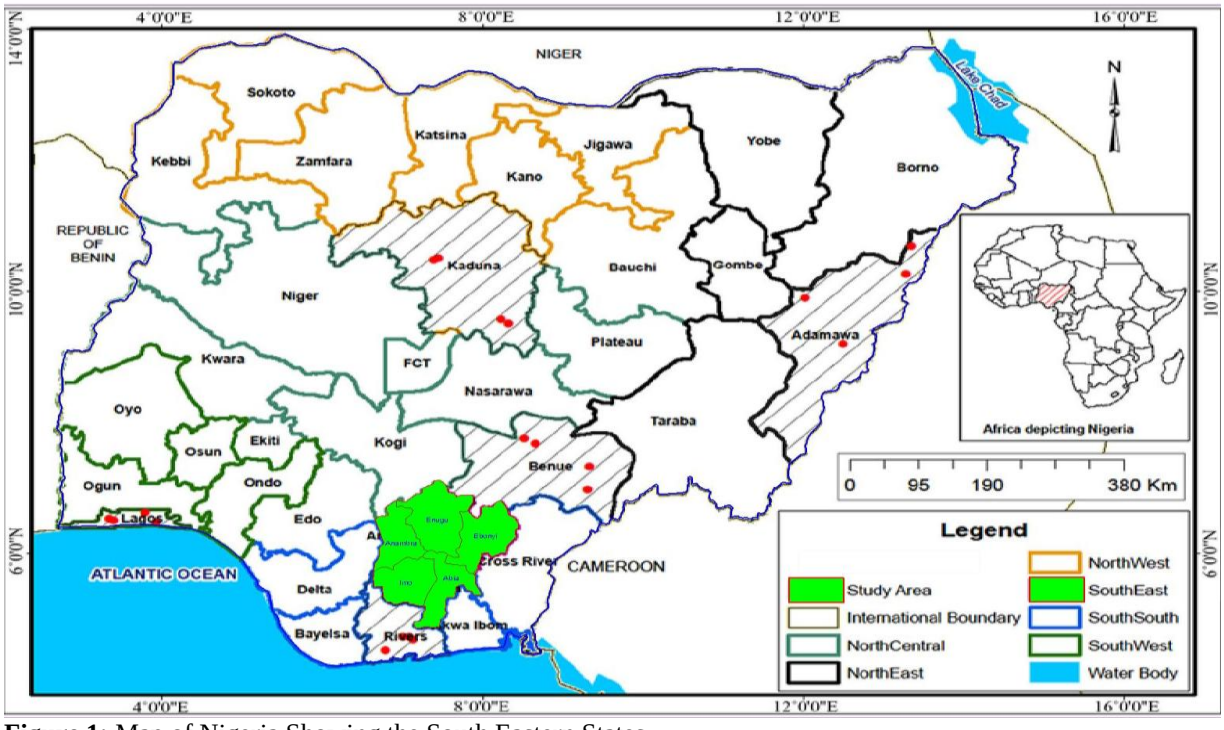

Figure 1: Map of Nigeria Showing the South Eastern States.
Source: google.com, Accessed 24/07/2015

IV. Data Presentation and Analysis

Two sets of data were collected for the study, namely, tourism potentials and accessibility.

4.1 Tourism Potentials in the South-Eastern Nigeria.

The tourism potentials that were sourced in the area were mostly such potentials that are of national importance. Some of the potentials are site based while there some that are event based. Event based tourism potentials come up during certain periods of the year and the location of such events may vary from year to year. The potentials are shown in Table 1.

Table 1: Tourism Potentials in the South-Eastern Nigeria.

S/N	State	Potentials	Remarks
1	Abia	i. Arochukwu cave ii. Long Juju of Arochukwu	Site attraction Event attraction
2	Anambra	i. Ogbunike Cave ii. Igbo Ukwu Archeological excavation	Site attraction Site attraction
3	Ebonyi	i. Ndibe Beach, Afikpo ii. Uburu Salt Lake iii. Abakaliki Green Lake	Site attraction Site attraction Site Attraction
4	Enugu	i. Opi Lake Complex ii. Ngwo Water Falls iii. Mmanwu Festival	Site attraction Site attraction Event attraction
5	Imo	i. Oguta Lake	Site attraction

Source: *Authors' Survey, 2015.*

In Table 1, of the eleven potentials of national recognition, nine are site based while two are event based.

4.2 Accessibility Characteristics in the South-East.

The ease with which the states are accessed, and the distances were explored. The ease was adjudged from personal experiences of the authors on one hand, and interview of other travelers in the zone, on the other hand. The experiences were based on ease of accessibility of the state capitals, namely Umuahia, Awka, Abakaliki, Enugu and Owerri. The assessment was categorized into three ratings and scores as follows:

i. Very good – 3: when the interconnection is entirely of tarred road that is in good repair.
ii. Good – 2: When the interconnection is of tarred road with minimal areas in disrepair; or not tarred but in good repair.
iii. Poor (1) when the interconnection is tarred and/or not tarred and in major disrepair.

The findings are shown in Table 2 while the major link routes are shown in Figure 2.

Table 2: Rating of Interconnectivity of the South-East States.

S/N	From	To	Distance (Km)	Rating	Score
1	Abakaliki	Awka	-	Poor	1
2	Abakaliki	Enugu	-	Very good	3
3	Abakaliki	Owerri	-	Good	2
4	Abakaliki	Umuahia	-	Good	2
5	Enugu	Awka	174	Good	2
6	Enugu	Owerri	152	Good	2
7	Enugu	umuahia	62	Poor	1
8	Awka	Awka	141	Poor	1
9	Awka	Umuahia	126	Poor	1
10	Owerri	Umuahia	83	Very good	3
Total Score					**18**
Average Score = 18/10 = 1.8					
Percentage Score = 100(18/30) = 60%					

Source: *Authors' survey, 2015.*

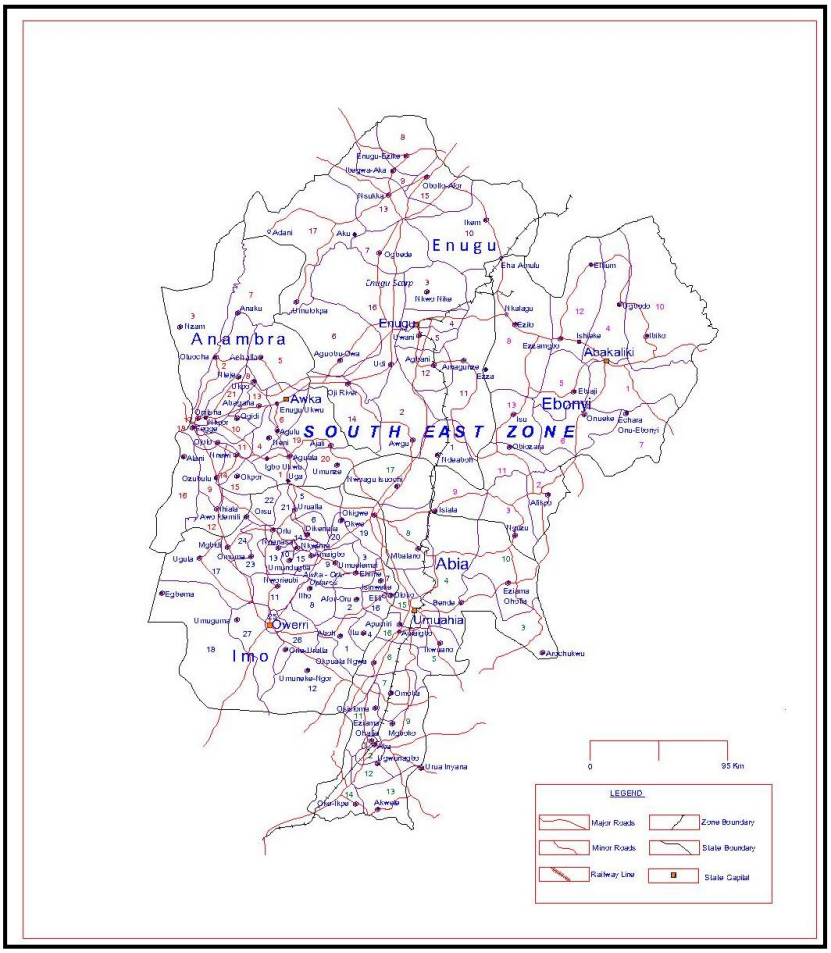

Figure 2: Transport Routes
Source: google.com, Accessed 24/07/2015

VI. Discussion of Findings

The identified tourism potentials in the South-East zone as shown in Table 1, as indicated earlier, are those ones which have been acclaimed to be of national significance. There are however, other site and event attractions which traverse the zone, and which when given attention will attain the status of national tourism sites and events. It is believed that any deliberate attention paid to such sites and events would make them approximate returns from the petroleum industry.

Data on interconnectivity of the different states in the zone as deduced from quality of the average rating of 1.8 depicts a situation that is below good standard. This can be said of other facilities. The routes that connect the state capitals depict similar physical characteristics. Whatever form of intervention on roads to enhance connectivity can be replicated in such other areas of tourism facilities as parking areas, railway lines, habours, airports, runways. Utility services like water supply, electricity supply, drainage and sewage disposal would also be included in any such intervention scheme. The intervention that best suits the quest of this study is one that is anchored on the Environmental Planning and Management (EPM) process.

6.1 EPM Process in Good Tourism Environment for the South East Zone

This section showcases an epitome of the strategies that are capable of engendering sustainable socio-spatial environment for tourism activities in the South-East geo-political zone of Nigeria, while adopting the EPM process. Three levels of operation of the process can be adopted. The levels include:

(i) Zonal Level-comprising the five states.
(ii) State Level- comprising the local government areas in each state.
(iii) Local Government Level- comprising the communities.

There will be a similar process for all the three levels. The difference will be on the composition of the stakeholders. At the zonal level, each of the states will be represented in a forum to be called the Zonal Tourism Forum (ZTF). Other stakeholders will include representatives from international and federal agencies that are

domiciled in any of the member states. The state representatives should be those in charge of Tourism Boards. ZTP will be coordinated by relatively qualified personnel in tourism matters. The appointment of the coordinator will be by the minister of the ministry in charge of tourism matters in Nigeria.

At state level, all the local governments will be represented in a forum to be called State Tourism Forum (STF). The representatives should be those that are charged with the responsibility of tourism matters in the local governments. Other stakeholders will comprise representatives from related ministries, tertiary institutions, non-governmental organizations (NGOs), trade unions and other related national and international agencies. The coordinator of the forum will be the officer in charge of the State Tourism Board.

At the local government level, the communities where tourism potentials exist will be represented in a forum to be called Local Tourism Forum (LTF). Other stakeholders will include representatives from community based organization (CBOs) faith based organization, trade unions and other related agencies. The co-ordinator will be the personnel incharge of the local government tourism committee.

At each level of the forum, the following steps will be followed to address any issue that is of tourism importance:

i. Identify, prioritize and clarify the tourism issues.
ii. Agree on methods, actions needed for the issues.
iii. Formulate plans with all necessary imports like finance.
iv. Institutionalize the process.

Tourism action plans from the local governments and states will be collated at the zonal level to form an action plan for the ZTP.

6.2 Areas of Operation

The objective of the Zonal Tourism Forum (ZTF) will be to achieve an all-round development of tourism sites as well as events in the South-East zone of Nigeria. The development will range from the known ones to those to be explored in the zone. The development will be in form of ensuring that the following items are in place:

i. Good roads to the sites
ii. Parking areas
iii. Airports and runways
iv. Water supply
v. Electricity supply
vi. Drainages and sewage
vii. Railway lines

The activities of ZTF will enhance private development of such other infrastructure as:

i. Passenger traffic terminals
ii. Hotels
iii. Restaurants
iv. Shopping facilities
v. Entertainment facilities
vi. Shopping facilities
vii. Telecommunications
viii. Taxis and buses.
ix. Commercial and other banks.

VII. Recommendations

The following recommendations are advanced with a view to achieving the objectives of this research work:

i. The fora advocated, Zonal Tourism Forum (ZTF), State Tourism Forum (STF) and the Local Tourism Forum (LTF) should be adopted and implemented to ensure a sustainable socio-spatial environment for tourism activities in the South-East zone of Nigeria. In those fora, the tenets of the EPM process as exposed by Wahab (1998) will be engendered in the zone.
ii. There should be an exhibition of political will on the parts of elected officials at the federal, state and local government levels to explore tourism as an economic venture. In this way, fiscal policies towards achieving the quest of this study will be frictionless.
iii. The entire process should be institutionalized by the concerned states in union with the federal government to enable follow-up actions in the operation of the process.

VIII. Conclusion

This study has shown the quality of the five states that make up the South-East zone to be formed into a unit of tourism location. The place of the EPM process in achieving this has also been addressed. Being a bottom-up approach to environmental planning, the process is capable of ensuring a smooth and frictionless way to ensuring a sustainable unit of tourism environment in the South-Eastern part of Nigeria.

References

[1] Bloxom, W. (1986) "The Sustainable Cities Programme and the Sustainable Ibadan Project". Ibadan; *EPM News*, Issue 1 Vol. 1 pp 1-2

[2] Iyi, E.A. and Ugwu, L.N. (2009) "Combating Adverse Effects on Oil Production and Distribution in the Niger Delta Region (NDR)". *Journal of Environment and Social Harmony* 2(1) Enugu. Faculty of Environmental Science, Enugu State University of Science and Technology. Pp. 173 – 182.

[3] Richardson B.R. (2010). The Contribution of Tourism to Economic Growth and Food Security, USAID Mali, Office of Economic Growth.

[4] UNCH/UNEP (1987) Environmental Guidelines for Settlements Planning and Management. Vol. Institutionalizing Environmental Planning and Management for Settlements Development, Nairobi.

[5] Wahab, B. (1998) "The Relevance of Environmental Planning and Management (EPM) Process to Local Government: The Case of Sustainable Ibadan Project" (SIP) Nigeria. *Journal of the Nigerian Institute of Town Planners*. Vol. XI. Pp. 12-29.

[6] World Travel and Tourism Council (WTTC) (2012). World Economic Impact Report, London.

ISSN (e): 2250 – 3005 || Volume, 05 || Issue, 11 ||November – 2015 ||
International Journal of Computational Engineering Research (IJCER)

Strong (Weak) Triple Connected Domination Number of a Fuzzy Graph

N.Sarala[1], T.Kavitha[2]
[1] Department of Mathematics, ADM College, Nagapattinam, Tamilnadu , India
[2] Department of Mathematics, EGSP Engineering College, Nagapattinam, Tamilnadu , India

ABSTRACT

A subset S of V of a nontrivial fuzzy graph G is said to be strong (weak) triple connected dominating set, if S is a strong (weak) dominating set and the induced sub graph <S> is a triple connected. The minimum cardinality taken over all strong (weak) triple connected dominating set is called the strong (weak) triple connected domination number and it denoted by γ_{stc} (γ_{wtc}).we introduce strong (weak) triple connected domination number of a fuzzy graphs and obtain some interesting results for this new parameter in fuzzy graphs.

Keywords: *Connected dominating set, Fuzzy graphs,triple connected dominating set, strong (weak) triple connected dominating set*

I. Introduction

In 1975, the notion of fuzzy graph and several fuzzy analogues of graph theoretical concepts such as paths cycles and connectedness are introduced by Rosenfeld[15] Bhattacharya[3] has established some connectivity regarding fuzzy cut node and fuzzy bridges. The concept of domination in fuzzy graphs are introduced by A.Somasudaram and S.Somasundaram[18] in 1998. In 2012, Bounds on connected domination in square of a graph is introduced by M.H.Muddabihal and G.Srinivasa.Triple connected domination number of a graph introduced by G.Mahadevan,Selvam. In this paper,We analyze bounds on strong (weak) triple connected dominating set of fuzzy graph and proves some results based on triple connected dominating fuzzy graph.

II.Preliminaries

Definition 2.1

A fuzzy subset of a nonempty set V is mapping $\sigma: V \to [0, 1]$ and A fuzzy relation on V is fuzzy subset of V x V. A fuzzy graph is a pair G: (σ,μ) where σ is a fuzzy subset of a set V and μ is a fuzzy relation on σ, where $\mu(u,v) \leq \sigma(u) \wedge \sigma(v)$ $\forall u,v \in V$

Definition 2.2

A fuzzy graph G=(σ, μ) is a strong fuzzy graph if $\mu(u,v) = \sigma(u) \wedge \sigma(v)$ for all u, $v \in V$ and is a complete fuzzy graph if $\mu(u,v) = \sigma(u) \wedge \sigma(v)$ for all u, $v \in V$.The complement of a fuzzy graphG=(σ, μ) is a fuzzy graph $\bar{G} = (\bar{\sigma}, \bar{\mu})$ where $\bar{\sigma}=\sigma$ and $\bar{\mu}(u,v) = \sigma(u) \wedge \sigma(v) - \mu(u,v)$ for all u, $v \in V$. we denote a cycle on P vertices by C_p, a path by P_p a complete graph on P vertices by K_p.

Definition 2.3

Let G=(σ, μ) be a fuzzy graph. Then $D \subseteq V$ is said to be a fuzzy dominating set of G if for every $v \in V-D$, There exists u in D such that $\mu(u,v) = \sigma(u) \wedge \sigma(v)$. The minimum scalar cardinality of D is called the fuzzy dominating number and is denoted by γ (G). Note that scalar cardinality of a fuzzy subsetD of V is $|D| = \sum_{v \in V} \sigma(v)$

Definition 2.4

A dominating set D of a fuzzy graph G = (σ, μ) is connected dominating set if the induced fuzzy sub graph <D> is connected. The minimum cardinality of a connected dominating set of G is called the connected domination number of G and is denoted by γ_c (G)

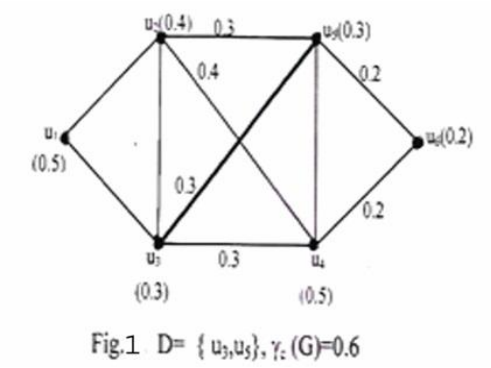

Fig.1 D= { u_3,u_5}, γ_c (G)=0.6

Definition 2.5

Let G be a fuzzy graph the neighborhood of a vertex *v* in V is defined by N(v) ={u∈V:μ (*u*,*v*) =σ (*u*) Λ σ (*v*)}.The scalar cardinality of N(V) is the neighborhood degree of V, Which is denoted by $d_{N(V)}$ and the effective degree of V is the sum of the weights of the edges incident on V denoted by $d_{E(v)}$

Definition2.6

Let u and v be any two vertices of a fuzzy graph G. Then u strongly dominates v(v weakly dominates u) if

i) μ (*u*,*v*) = σ (*u*) Λσ (*v*). and
ii) $d_{N(u)} > d_{N(v)}$

Definition2.7

Let G be a fuzzy graph, then D ⊆V is said to be a strong(weak) fuzzy dominating set of G if every vertex v∈V-D is strongly (weakly) dominated by some vertex u in D. We denoted a strong (weak) fuzzy dominating set by sfd -set(wfd-set).

The minimum scalar cardinality of a sfd-set(wfd-set) is called the strong (weak) fuzzy domination number of G and it is denoted by γ_{sd}(G) (γ_{wd}(G))

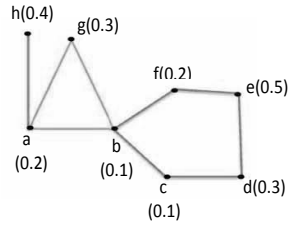

Fig:2

Example2.8

For the fuzzy graph G in Fig.2.γ_{sd}(G) =0.8 and γ_{wd}(G)=1.0.since {a,b,e} and {c,f,g,h} are the minimum sfd-set and wfd-set respectively.

Theorem 2.9

Let D be a minimal sfd- set of a fuzzy graph G. Then for each u∈D of the following holds.

(i) No vertex in D strongly dominate v
(ii) There exists v∈ V-D such that v is the only vertex in D which strongly dominates u.

Proof

Suppose D is a minimal connected dominating set of G. Then for each node u∈D the set D′=D-{u} is not a connected dominating set. Thus, there is a node v∈V-D′ which is not dominated by any node in D′. Now either u=v or v∈V-D, If v=u then no vertex in D strongly dominates v. If v∈V-D and v is not dominated by D-{u} but is dominated by D, Then u is the only strong neighbor of v and v is the only vertex in D which strongly dominates u.

Conversely suppose D is a dominating set and each node u∈D, one of the two stated conditions holds. Now we prove D is a minimal strong connected dominating set. Suppose D is not a minimal strong connected dominating set, then there exists a node u∈D such that D-{u} is a dominating set. Therefore condition (i) does not hold. Also if D-{u} is a dominating set then every node in V-D is a strong neighbor to at least one node in

D-{u}. Therefore condition (ii) does not hold. Hence neither condition (i) nor (ii) holds which is a contradiction.

Definition2.10
A fuzzy graph G is said to be triple connected if any three vertices lie on a path in G. All paths, cycles, complete graphs are some standard examples of triple connected fuzzy graphs.

Definition2.11
A subset D of V of a nontrivial connected fuzzy graph G is said to be triple connected dominating set. If D is the dominating set and the induced fuzzy sub graph <D> is triple connected .The minimum cardinality taken over all triple connected dominating set of G is called the triple connected dominating number of G and is denoted by $\gamma_{tc}(G)$.

Example 2.12
For the fuzzy graph Fig.3, D = $\{v_1,v_2,v_5\}$ forms a γ_{tc} set of G

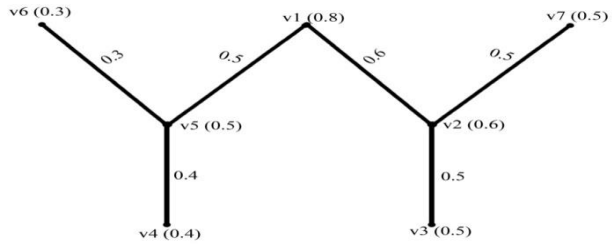

Fig.3, $\gamma_{tc}(G)$ =0.8+0.5+0.6 =1.9

III.Strong (weak) Triple connected domination number of a fuzzy graph

Definition3.1
A subset S of V of a nontrivial fuzzy graph G is said to be strong (weak) triple connected dominating set, if S is a strong (weak) dominating set and the induced sub graph <S> is a triple connected. The minimum cardinality taken over all strong (weak) triple connected dominating set is called the strong (weak) triple connected domination number and it denoted by γ_{stc} (γ_{wtc}). In this section we present few elementary bounds on strong(weak) triple connected domination number of a fuzzy graph and the correspondingsome results

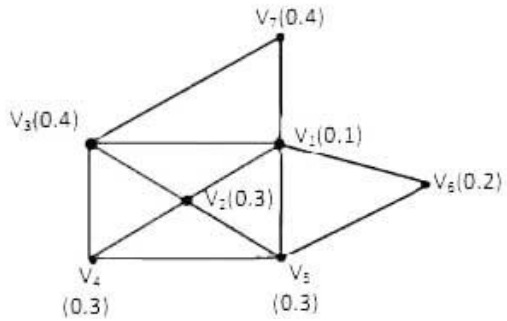

Fig:4

Example3.2 For the fuzzy graph in Fig : 4, s = **{**v_1,v_2,v_6**}** forms γ_{stc} set and w = $\{v_3,v_4,v_5\}$ formsγ_{wtc} set.
$\gamma_{stc}(G) = 0.6$ and $\gamma_{wtc}(G) = 1$
Theorem3.3
Strong (weak) triple connected dominating set does not exists for all fuzzy graphs.
Proof By definition,The connected graph is not strong (weak) triple connected.consider only connected fuzzy graphs for which strong (weak) triple connected dominating set exists.
Observation 3.4 Every strong (weak) triple connected dominating set is a dominating set but not conversely.
Observation 3.5 Every strong (weak) triple connected dominating set is a triple connected dominating set but not conversely.
Observation 3.6 The complement of strong (weak) triple connected dominating set need not be a strong (weak) triple connected dominating set.

Theorem3.7 For a fuzzy graph G of order p, **(**i) $\gamma(G) \leq \gamma_{sd}(G) \leq \gamma_{stc}(G)$ $P\text{-}\Delta_N(G) \leq p\text{-}\Delta_E(G)$ and
(ii) $\gamma(G) \leq \gamma_{wd}(G) \leq \gamma_{wtc}(G) \leq P\text{-}\delta_N(G) \leq p\text{-}\delta_E(G)$ where $\Delta_N(G)$ $[\Delta_E(G)]$ and $\delta_N(G)$ $[\delta_E(G)]$ denote the maximum and minimum neighborhood degrees (effective degrees)of G

Proof Since every stcd set (wtcd) is a fuzzy dominating set of G, $\gamma(G) \leq \gamma_{sd}(G) \leq \gamma_{stc}(G)$ and $\gamma(G) \leq \gamma_{wd}(G) \leq \gamma_{wtc}(G)$.Let u ,v∈V, If $d_{N(u)} = \Delta_N(G)$ and $d_{N(v)} = \delta_N(G)$.Then clearly V-N(u) is a stcd- set and V-N(v) is a wtcd -set. Therefore $\gamma_{stc}(G) \leq |V\text{-}N(u)|$ and $\gamma_{wtc}(G) \leq |V\text{-}N(u)|$ that is $\gamma_{stc}(G) \leq P\text{-}\Delta_N(G)$ and $\gamma_{wtc}(G) \leq P\text{-}\delta_N(G)$ Further since $\Delta_E(G)] \leq \Delta_N(G)$and $\delta_E(G) \leq \delta_N(G)$

Hence $\gamma(G) \leq \gamma_{sd}(G) \leq \gamma_{stc}(G) \leq P\text{-}\Delta_N(G) \leq p\text{-}\Delta_E(G)$ and $\gamma(G) \leq \gamma_{wd}(G) \leq \gamma_{wtc}(G) \leq P\text{-}\delta_N(G) \leq p\text{-}\delta_E(G)$

Theorem3.8 For any connected fuzzy graph G, $\gamma(G) \leq \gamma_c(G) \leq \gamma_{tc}(G) \leq \gamma_{stc}(G) \leq \gamma_{wtc}(G)$.

Proof Let G be a fuzzy graph and D be a minimum dominating set. D_{tc} is triple connected dominating set but need not be a minimum fuzzy dominating set, and alsoD_{stc} is a strong (weak) triple connected dominating set.

Therefore we get$|D| \leq |D_c| \leq |D_{tc}| \leq |D_{st}|$ and$|D_{stc}| \leq |D_{wtc}|$

That is $\gamma(G) \leq \gamma_c(G) \leq \gamma_{tc}(G) \leq \gamma_{stc}(G) \leq \gamma_{wtc}(G)$.

Theorem 3.9 If a spanning sub graph H of a graph G has a strong(weak) triple connected dominating set then G also has a strong (weak) triple connected dominating set.

Proof Let G be a connected fuzzy graph and H is the spanning sub graph of G. H has a strong (weak) triple connected dominating set and V(G) = V(H) therefore G is a strong (weak) triple connected dominating set.

Theorem 3.10 For any connected fuzzy graph G with P vertices and strong (weak) triple connected dominating vertices P if any only if $G \cong P_3$ or C_3.

Proof Suppose $G \cong P_3$, C_3 then the strong(weak) triple connected dominating vertices is 3, and P vertices. Conversely, Let G be a connected fuzzy graph with P vertices such that strong (weak) triple connected dominating vertices P then

$G \cong P_3$ or C_3

Theorem 3.11 For any connected fuzzy graph G with P≥3 vertices and exactly one vertex has$\Delta_N(G) \leq P\text{-}2$, the strong triple connected dominating vertices is 3.

Proof Let G be a connected graph with P≥3 vertices and exactly one vertex has maximum neighborhood degree $\Delta_N(G) \leq P\text{-}2$.Let v be the vertex of maximum neighborhood degree $\Delta_N(G) \leq P\text{-}2$. Let $v_1, v_2 \ldots\ldots$ and v_{p-2} be the vertices which are adjacent to v and Let v_{p-1} be the vertex which is not adjacent to v. Since G is connected, v_{p-1} is adjacent to a vertex v_i for some i, Then $s = \{v, v_i, v_{p-1}\}$ forms a minimum strong triple connected dominating set of G.

Theorem 3.12 For a connected fuzzy graph G with 5 vertices, the strong triple connected dominating vertices is P-2 if and only if G is isomorphic to P_5, C_5.

Proof Suppose G is isomorphic to P_5, C_5then clearly strong triple connected dominating vertices is P-2 conversely, let G be a connected fuzzy graph with 5 vertices and strong triple connected dominating vertices is 3. Let $S=\{ v_1, v_2, v_3\}$ be a γ_{stc} set then clearly <S> = P_3 or C_3. Let V-S= V(G)-V(S)= $\{ v_4, v_5 \}$ then

{V-S} =K_2 or $\overline{k_2}$

Case (i)<S> = $P_3 = v_1 v_2 v_3$

Sub case (i)<V-S> = $K_2 = v_4 v_5$

Since G is connected, there exists a vertex say v_1 (or v_3) in P_3 which is adjacent to v_4 (or v_5) in K_2, then $s=\{v_1, v_2, v_4\}$ forms γ_{stc} set of G so that strong triple connected dominating vertices is P-2. If v_4 is adjacent to v_1, if the vertices v_1 and v_2 are connected to two vertices, v_3 is connected to one vertex then G is isomorphic to P_5. Since G is connected there exists a vertex say v_2 in P_3 is adjacent to v_4 (or v_5) in K_2. Then $S=\{ v_2, v_4, v_5\}$ forms a γ_{stc} set of G so that strong triple connected dominating vertices is P-2. If the vertex v_1 and v_3 are connected to two vertices and v_2 is connected to one vertex. Then G is isomorphic to P_4. Now by increasing the degree of the vertices by the above arguments, we have $G \cong C_5$

subcase (ii)<V-S> = $\overline{k_2}$.

Since G is connected, then there exists a vertex say v_1(or v_3) in P_3 is adjacent to v_4 and v_5 in $\overline{k_2}$. Then $S=\{ v_1, v_2, v_3\}$ forms a γ_{stc} set of G so that strong triple connected dominating vertices is P-2. Since G is connected. There exists a vertex say v_2 in P_3 which is adjacent to $v_4$and v_5 in $\overline{k_2}$. Then $S=\{ v_1, v_2, v_3\}$ forms a γ_{stc} set of G so that strong triple connected dominating vertices is P-2.since G is connected, there exists a vertex say v_1 in P_3 which is adjacent v_2 in $\overline{k_2}$ and v_3 in P_3 is adjacent to v_5 in K_2. Then $S=\{ v_1, v_2, v_3\}$ form a γ_{stc} set of G so that strong triple connected dominating vertices is P-2. Since G is connected, then there exists a vertex

say v_1 in P_3 is adjacent to v_4 in $\overline{k_2}$ and v_3 in P_3 is adjacent to v_5 in $\overline{k_2}$. Then S={ v_1,v_2 ,v_3} forms a γ_{stc} set of G so that strong triple connected dominating vertices is P-2

Case (ii)<S> = C_3= v_1v_2 v_3 v_1
Sub case (i)<V-S>= K_2 = v_4v_5
Since G is connected, there exists a vertex say v_1, (or v_2 ,v_3) in C_3 is adjacent to v_4 (or v_5). Then S={ v_1,v_2 ,v_4} forms a γ_{stc} set of G so that strong triple connected dominating vertices is P-2. If the vertex v_1, v_2, and v_3 are connected to two vertices than G ≅ C3
Sub case (ii)<V-S> = K_2

Since G is connected there exists a vertex say v_1(or v_2 ,v_3) in C_3 is adjacent to v_4 in $\overline{k_2}$ and v_2 (or v_3) in C_3 is adjacent to v_5 in $\overline{k_2}$. Then S={ v_1,v_2 ,v_3} forms aγ_{stc} set of G so that strong triple connected dominating vertices is P-2.

IV. Conclusion

The strong (weak) triple connected domination number of fuzzy a graph is defined. Theorems related to this concept are derived and the relation between triple connected domination number of fuzzy graphs and strong (weak) triple connected domination number of fuzzy graphs are established.

References

[1] AntonyXaviorD,FlorenceIsido D, Chitra V.M., On Domination in Fuzzy graph,Inter.journal of com.Algorithm vol 02(2013), 248-250.
[2] Bhutani K.R, Strong arc in Fuzzy graphs, Information science,152(1989),319-322.
[3] Bhattacharya, Some remarks on fuzzy Graphs,PatterRecognition letter 6(1987), 297-302.
[4] HararyF (1972),Graph Theory,Adisen-wesley Reading mass.
[5] Haynes T.W.,Headetniemi S.T., Slater P.J, Fundanmental Domination in Graph,MarcelDekkeel,Newyork
[6] Laura A.sanchis,On the number of edges in graph with a given connected domination number,Elsevier,Discrete Mathematics 214(2000) ,193-210.
[7] Moderson N. and Nair P.S., Fuzzy graphs and Fuzzy Hyper graphs, Physicaverlag(2000).
[8] Muddebihal M.H., SrinivasaG, Bounds connected domination in squares of graph ,Inter.Jour.sci. andTech.vol 1.No.4(2012),170-175
[9] Mahadevan G.,Selvam. Triple connected complementary Tree domination number of a graph. International Mathematics Forum,Vol.8,2013,no.14,659-670
[10]. MahadevanG,Selvam. Triple connected domination number of a graph. International Mathematics Combin,Vol.3,2012,93-104
[11] MahadevanG,Selvam,BhagavathyAmmal, Avadayappan,Subramanian.T, Strong Triple connected domination number of a graph. IJCER Vol.3(2013) 242-247
[12] MahadevanG,Selvam,BhagavathyAmmal, Avadayappan,Subramanian.TWeak Triple connected domination number of a graph. IJMER Vol.3(2013) 342-345
[13] NagorGaniA.andchandrasekaran V.T, Domination in Fuzzy graph, Advances in Fuzzy sets and system1 (1)(2006), 17-26.
[14] *Natrajan.C,AyyaswamyS.K, On strong (weak) domination in fuzzy graph, World academy of sci.Engineering Technology Vol 43(2010)526-528*
[15] RosenfeldLA..ZedehA,FuK.S.Tanaka .K.,M.Shimura(Eds) ,Fuzzy sets and their Application to cogenitive and Decision Processes, Academic press, Newyork (1975) ,77-95
[16] Sarala.N,kavitha,T.,Triple connected domination number of fuzzy graph, International Journal of Applied Engineering Research, Vol. 10 No.51 (2015)914-917
[17] Sarala.N, kavitha, T.,Connected Domination Number of Square Fuzzy Graph,IOSR-JM, Volume 10, Issue 6 Vel III (2014), 12-15.
[18] Somasundaram.A.and.Somasundaram .S,DominationinFuzzy graph-I.,Pattern Recognitionletter19(9) (1998)77-95.

ISSN (e): 2250 – 3005 || Volume, 05 || Issue, 11 ||November – 2015 ||
International Journal of Computational Engineering Research (IJCER)

Development of a Cassava Starch Extraction Machine

[1*]Olutayo, L. A; [1]Mogaji K.O and [1]Fasoyin S.A
[1]*Department of Agricultural and Bio-Environmental Engineering Technology, Rufus Giwa Polytechnic, Owo, Ondo-state, Nigeria*

ABSTRACT
Cassava starch extraction machine that is easy to assemble, operate and maintain was developed and tested. The major components of the machine are hopper, mixing unit, extraction chamber which houses the screw conveyor (auger) and sieve, discharge outlets and the power unit. The machine was powered by 2 Kw electric motor. The working principle of the machine is by feeding cassava mash and water through the hopper, under gravity they both fall freely into the mixing unit, the rotated stirrers mixed the mash and water properly before it is discharged to the extraction chamber where the screw conveyor move and rotates it over a sieve thereby causing the moist starch to viberate.The machine was tested with 5kg TMS 30572 cassava mash with different water quantity (10 – 22)litres. It was observed that at 18litres of water and 120rpm stirrers speed. The output capacity was 25.2kg/hr and the extraction efficiency was 80%. The total cost of production of the machine was ₦86,400.00. The machine is recommended for small and medium producers of cassava starch.

Keywords: *Development, cassava starch, extraction, machine, production cost*

I. INTRODUCTION

Cassava (*manihotesculentacrantz*) is a perennial tuber plant widely grown in many tropical countries including Nigeria (Adejumo, *et al*, 2011). Olukunle, (2005) reported that cassava is a major source of carbohydrate in most developing nations of the world. Sheriff, *et al*, (2005) described cassava as a wonder crop due to its potential use in several agro and agro-allied industries. Since 1990 Nigeria has surpassed Brazil as the world's leading producer of cassava with an estimated annual production of 54 million metric tons from 30million hectares of land (FAO, 2012). Starch is a polymer of glucose found in most plant (Thebaudin, *et al*, 2005). It is produced from various plants or crops like potatoes, cassava roots, rice, wheat etc. Starch is one of the most abundant substances in nature, it is almost unlimited resources. Starch is used as food (Sriroth and Peterson, 2000) it is also used to produce diverse products like textiles, adhesives; pharmaceuticals etc. Cassava starch is preferred amongst other starches because of its gelling property. FAO (2007) captioned cassava starch as native and modified starches. It is native starch when it is produced by the separation of natural occurrence, like starch from cassava roots can be use directly to produce certain food, such as noodles. While modified starch is a native starch that has been changed in its physical or chemical properties.. Modified starches are needed to improve textural paste and gels and also to modify cooking characteristics.

Starch production in Nigeria is dominated by cottage industries (Olukunleand Olukunle, 2007). Adepomola, (2004) identified ten large scale starch industries in Nigeria, Only one (Matna food company, Ogbese, Ondo state, Nigeria) is functional. The survey conducted by Adepomola, (2004) reported by Olukunle and Olukunle (2007) shows that the processing of cassava to starch is largely done using traditional or manual method.

Olukunle and Olukunle (2007) designed a cassava starch extractor, which is a modification of a fruit juice extractor. The machine consists of the milling/extraction mechanism, the transmission system, the upper half of the extraction chamber (cage), the perforated lower half of the extraction chamber (basket), the hopper, water pump and water delivery system, fiber outlet and the starch collector. The machine mills the peeled cassava tubers and conveys the mash into a stream of water flowing with high pressure; starch is separated through the perforated concave into the starch sedimentation tank.

Godwin (2013), said that the small- to medium scale production of starch in Brazil is schematically similar to that of starch in Colombia, He described that fresh roots cassava are delivered to the plant and fed into a rotary washer fitted with overhead water sprays for part of its length. As well as washing off dirt and debris, the tumbling action of the roots as they pass along the washer also removes most of the bark. Washed roots are transferred to the hopper-feed, roof disintegrator, via an inspection conveyor, at which an operator cuts up excessively large roots and removes remaining bark and stems.

(Grace, 2003) also designed a cassava starch extraction machine, this machine consist of a hollow cylindrical drum with tooth – edged steel blades sandwiched between local hardwood slats fixed longitudinally to its surface. The drum is mounted between two circular steel endplates on a central shaft and housed inside a steel casing, the base of which includes a screening plate. Recycled liquor from starch separators is continuously fed into the disintegrator. The resultant slurry of crushed roots passes through the screening plate into a sump tank from which it is pumped to the separators.

Bruinsma*et al.* (2001) designed two-stage separation cassava starch extraction machine. This is used to remove the liberated starch from the fibrous pulp (Massa). These employ two centrifugal separators, which have replaced the traditional rotating brush – and – screen washers. The centrifugal separator consists of a rotating conical screen, housed inside a shaped mild – steel casing, tapering from front to back the conical screen is a metal frame covered with a nylon mesh. The narrow end of the cone is closed with a fixed metal plate connected to the drive shaft. Slurry is pumped into the center of the separator (toward the fixed plate) and forced through the screen to an outlet at the bottom of the casing into a sump tank. Water is spraying into the slurry from jets positioned around the screen. In the sump tank, the slurry receives extra water to facilitate pumping it over aflatbed reciprocating screen to remove any remaining fiber (large plants employ an additional centrifugal separator). The slurry then enters second separator for further starch extraction. Liquor discharged from the second separator is returned to the disintegrator and the suspension of pulp or "starch milk: is discharged to storage tanks.

Trim, *et al*. (2003) reported his cassava starch extraction machine dimensions for the channels vary considerably from plant to plant; in length ranged from 150 m to 200m; in width, 0.6 m to 1.0m and depth ranged from 0.4 m to 0.6m. The channels are usually lined with ceramic tiles because both starch and starch milk attack concrete. The channels are roofed to protect the starch from rain or direct sunlight. After fermentation, the starch is removed from the tanks, broken up with a spike mill and dried on hessian sacks laid on raised drying tables usually made of bamboo. The drying starch is agitated manually at regular intervals. When dry, the starch is collected, milled to a powder and packaged into bags.

In India, tanks are used instead of channels for sedimentation, because of historical reasons. After overnight settling and removal of the supernatant liquor, the starch cake had a concentration of solids at 50%, but after washing, the concentration was 55%, starch and crude fiber concentrations of the settled cake in two plants were similar, averaging 96.7% for starch and 0.3% for crude fiber (dry matter basis). The changes occurring in the starch, this is as a result of fermentation which is the subject of much recent research (Kurmi and Guptal, 2005). Although a minimum fermentation time of 30days is necessary, starch often remained in the tanks at the two plants for longer periods because of the lack of available drying space. Such prolonged fermentation had no detrimental effect on starch quality. The temperature of the fermenting starch at the two plants ranged between 12^0C and 13^0C.

However, then new technologies have been introduced and existing ones improved, to increase processing efficiency and open new markets for both cassava starch and flour. These new technologies include improved equipment for starch processing includesrappers with saws, continuous flow washer-pesters, vibrating screens and sedimentation channels.

II. MATERIALS AND METHODS

2.1 Design Machine Features

The machine (plate 1.) consists essentially of the following components; mixing unit, extraction chamber, discharge unit, frame and power unit.

2.1.1 The Hopper

This is the unit where the input materials (cassava mash and water) are fed into the machine. It is constructed with Galvanized Iron Sheet gauge 14

2.1.2 Mixing Unit

This unit consists of 16 stirrers attached to a single solid shaft. It is use for proper mixing of cassava mash and water.

2.1.3 Extraction Chamber

This consists of screw conveyor (auger) and sieve, the conveyor moves and rotates the diluted mash over a sieve thereby causing the moist starch to liberate.

2.1.4 Discharge units

This is where the moist starch and chaff are discharged out it is constructed with Galvanized Iron Sheet gauge 14.

2.1.5 Frame

This unit bears the load of the machine. It is also give support to the machine during operation. It is made from 150mm angle iron.

2.1.6 Power Unit

This unit supplied power that rotates both the stirrers and the screw conveyor with 2Kw electric motor through chain and sprocket

Plate 1: Pictorial view of cassava starch extraction machine

2.2 Operational Principle of the Machine

Cassava mash and water were fed into the machine through the hopper, under gravity the cassava mash water fall freely into the mixing unit, power was provided by an electric motor, which drive the stirrers and the screw conveyor, the rotated stirrers mixed the cassava mash and water properly to a desirable cassava mash : water ratio, the diluted cassava mash is discharge through the stopper to the extraction unit where the conveyor move and rotates it from one end to the other over a sieve thereby causing the moist starch to liberate through the sieve and the chaff is also discharge at the other outlet.

2.3 Design Analysis

The major designs were on the feeding chute, stirrers, screw conveyor, shaft selection, and power requirement.

2.3.1 Feeding Chute

The cassava starch extraction machine is expected to have a 30kg/hr. therefore, a hopper that is a pyramidal frustum with 45^0 angle of inclination was selected, with top opening of 400mm x 400mm, bottom opening of 150mm x 150mm and a side length of 200mm, angle 45^0 was used for the inclination to allow easy flow of the input material.

$$\alpha = tan^{-1}\mu \quad ---------- (1)\,(Kolawole, 2012)$$

α= angle of inclination and μ = co-efficient of friction of cassava mash

2.3.2 Stirrers/Mixing Unit

16 stirrers were attached to a single solid shaft for proper mixing of cassava mash and water.

F_t and F_s are two forces acting on the stirrers

$$F_t = \frac{MV^2}{r} \; and \; F_s = F_t tan\theta \quad ---------- (2)\,(Hall, etal, 1980)$$

Where,

M = mass of the stirrer, V = velocity, r = radius and $\theta = 20^0$

2.3.3 Screw Conveyor

The conveyor moves and rotates the diluted mash over a sieve thereby causing the moist starch to liberate.

Capacity of the conveyor $Q = \pi D^2 Sn\Psi\rho C \quad ----- (3)(Halletal, 1980)$

Where,

D = Screw diameter, S= Pitch, n = speed, Ψ = loading efficiency ρ = Bulk density and c = Factor for inclination to horizontal

2.3.4 Power requirement

The power requirement of the machine was determine with the expression by Khurmi and Gupta (2005)

$$P = \frac{2\pi nT}{60} \quad ---------- (4)$$

Where, P = power (watt), n = shaft speed (rpm) and T = torque required to turn the shaft.

Therefore, an electric motor of 2Kw (2hp) was selected.

2.3.5 Shaft Selection

The diameter of the shaft used was selected using the expression by (Hall et al, 1980)

$$D^3 = \frac{16}{\pi S_s}\sqrt{(K_b M_b)^2 + (K_t M_t)^2} \quad ----------(5)$$

Where,

D = Diameter of the shaft (mm), Ss = Allowable stress, 40 x 10^6N/m^2

M_b = Maximum bending moment, 1051.26Nm, M_t = Maximum torsional moment, 136.05Nm, K_b = Shock and fatigue to bending moment, 2.0, K_t = Shock andfatigue factor to torsional moment, 1.5 calculated shaft diameter was 34.60mm.

Therefore shaft of 35mm was selected for both.

2.4 Machine Production Cost

The production cost of cassava starch extraction machine was given under the following sub-heading below. It was calculated by using the concept of labour and machine hour rate (Godwin, 2013) for the overall production process involved in the fabrication of the machine.

i. the cost of Bought-Out components, ₦40,500
ii. the cost of materials, ₦30,200
iii. the cost of machining jobs, ₦10,500
iv. the cost of non-machining jobs, ₦5,200

The total cost of the production was ₦86, 400k

2.5 Test Procedure

The machine was tested following these procedures

i. 5Kg of TMS 30572 cassava mash was prepared at different quantity (10- 22) litres of water

ii. The weight of the mash and water input into the machine

3 The weight of the starch and chaff discharges after oven dried at 10.08 moisture content was also recorded.

4 The duration for each operation was noted.

III. RESULTS AND DISCUSSIONS

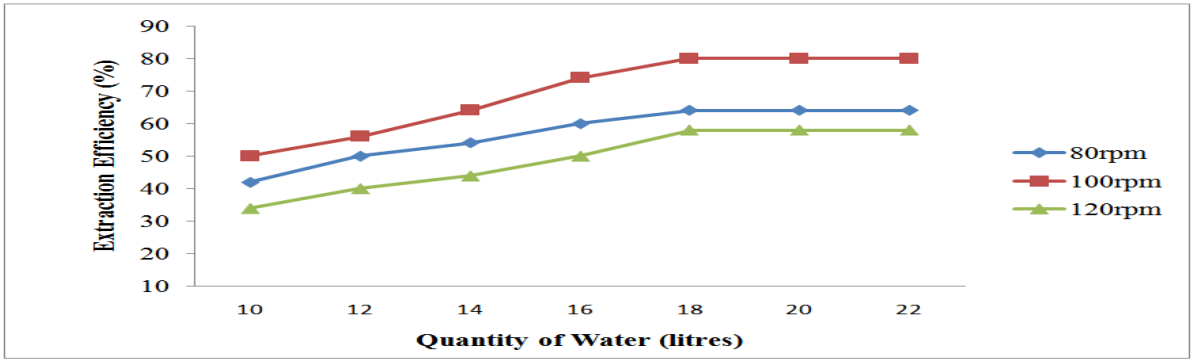

Fig. 1: Effect of stirrers' speed and water quantity on extraction efficiency

3.1. Performance Evaluation of the Machine

In Fig. 1, it was observed that the extraction efficiency for 80rpm stirrers speed ranged from 42% to 64%, whereas it was 50% and 80% extraction efficiencies for 100rpm while the extraction efficiency for 120rpm stirrers speed ranged from 34% to 58%.

Therefore, it can be deduced from the foregoing that the stirrers speed of 100rpm with appropriate water quantity of 18 litres have a significant effect on the extraction performance of the machine. Figure 1 shows view of the machine.

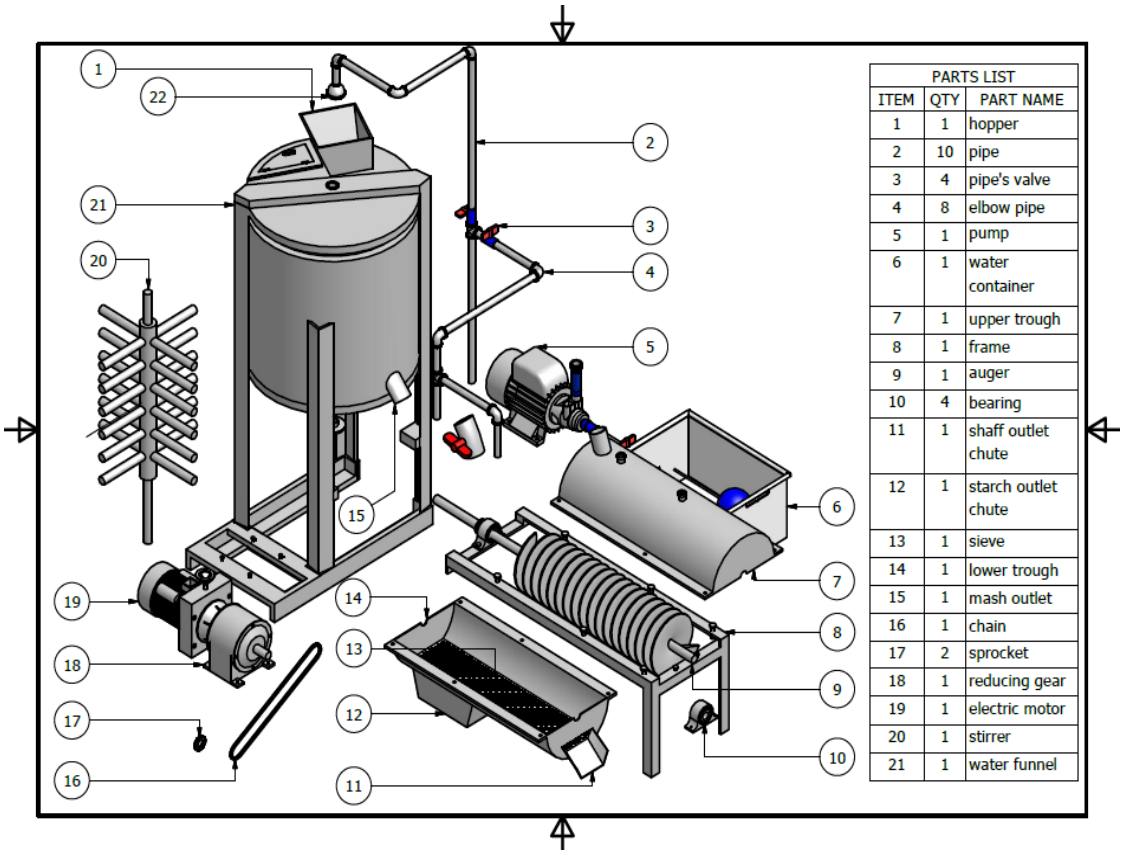

PARTS LIST		
ITEM	QTY	PART NAME
1	1	hopper
2	10	pipe
3	4	pipe's valve
4	8	elbow pipe
5	1	pump
6	1	water container
7	1	upper trough
8	1	frame
9	1	auger
10	4	bearing
11	1	shaff outlet chute
12	1	starch outlet chute
13	1	sieve
14	1	lower trough
15	1	mash outlet
16	1	chain
17	2	sprocket
18	1	reducing gear
19	1	electric motor
20	1	stirrer
21	1	water funnel

Figure 1: Exploded View of the Machine

IV. CONCLUSIONS

A cassava starch extraction machine was developed and evaluated. The machine had an output capacity of 20.2kg/hrwith extraction efficiency of 80%. A 3.5kg dried starch was obtained from 5kg TMS 30572 cassava mash. The highest starch discharged was obtained when the stirrers speed was 120 rpm and 18 litres

REFERENCES

[1] Adejumo A.L, Aderibigbe A.F and Layokun S.K (2011). Cassava Starch Production, Physic Chemical Property and Hydroxylation. Journal of Advance in food and Energy Security 2 (20011) Pp. 8-17 Anon (2008) "world food programmed" http:/ www.fao.com paper presented at International Starch Convention, 11-14 June 2004, Cracow, Poland.

[2] Adepomola, (2004). Development of a sustainable system for cassava starch Extractionagriculture organization of the united nation (FAO), Rome. Pp 155.

[3] Bruinsma, D. H; Witsenburg, W. W and Wurdemann, W. (2001). Cassava in selection of Canada Pp. 26 – 32.Cassava Starch Production in India. Paper presented at the International SymposiumsChouinard, A: Cassava Harvesting and Processing Proceeding of a workshop held at CIAT, Cali Colombia International Development Research Centre (IDRC), Ottawa,

[4] FAO (2007).Production Year Book for 2006, Rome, Food and Agriculture Organization, U.K.

[5] FAO (2012). Seventh International meeting on Cassava Breeding Bio technology and Ecology "Cassava Improvement to enhance livelihood in sub- Saharan African and North eastern Brazil "Brazil 11-15 Pp 102

[6] Godwin E.K (2013). Personal Communication E.K Engineering Tools and Equipment. IsoloLagos, Nigeria.

[7] Grace, M. R (2003).Cassava processing. FAO plant production and protection series food and

[8] Hall A.S., Holowenko A.R and Laughlin H.G (1980). Theory and Problems of machine design S.I metric Edition. McGraw – Hill Book Company, New York Pp 115.

[9] Kolawole O.P (2012). Development and Evaluation of cassava mash process Handling Machine Ph.D Thesis, Agricultural Engineering Department FUTA, Nigeria.

[10] Kurmi R.S and GuptaJ.K (2005). A Textbook of Machine Design. 15thEdition.Schand and Company Ltd. New Delhi, India.

[11] Olukunle O.J (2005).Development of a cassava Peeling machine. Conference on International Agriculture Research for Development Stuttgart- Holenheim, Oct. 11-13, 2005.

[12] Olukunle, O. J and Olukunle, O. F, (2007). Development of a sustainable system for cassava Production Sweet and Sour Starch in Colombia. In Weber, E. J. Cock, J. H and publishing and documentation (PUDDC), Wageningen the Netherlands P. 113 – 158

[13] Sherriff J.T, Kurup G.T and Nanda S.K (2005).Performance Evaluation of a Cassava Peeling Machine Journal of root Crops 2(11) Pp 30-35.

[14] Sriroth G.H and Peterson R.K (2000)."World Programmed on cassava production, http;//www.Fao.com.starch extraction, conference on international Agricultural Research for Development Technology for food processing in developing countries centre for agriculture

[15] Thebaudin J.Y, Lefebvre A.C and Doublier J.L (2005). Rheology of Starch Pastes from Starches of different Origin, Application to Starch based Sauces, leanese- wiss U-techno vol. 31, 354 -360.

[16] Trim, D. S; Nanda, S. K; Curran, A. Anantharaman, M; and Nair, J. (2003). Investigation of Trope tag 2007.Tropical Root Crops 6-9 Nov. Thiruvananthapuram, India.University of Kassel – witzennausen and University of Gottingen, October 9 – 11, 2007

ISSN (e): 2250 – 3005 || Volume, 05 || Issue, 11 ||November – 2015 ||
International Journal of Computational Engineering Research (IJCER)

The Myth of Softening behavior of the Cohesive Zone Model Exact derivation of yield drop behavior of wood

T.A.C.M. van der Put
TU Delft, Civil Engineering and Geosciences; Timber structures and wood technology -

Abstract:
It is shown that the postulate of strain softening of the fracture stress is based on the error to regard the nominal stress to be the actual, ultimate stress, at the actual area of the fracture plan. Strain softening called yield drop is elastic unloading of the actual elastic stress at the intact, not ltimate, elastic loaded part of the specimen, outside the fracture zone. It appears that the Griffith theory only applies for the first yield drop until half unloading and further fracture follows from a ultimate stress criterion A small-crack merging mechanism explains precisely the "softening" called yield drop curve.

Keywords: *wood, timber, fracture mechanics, limit analysis, strain softening, yield drop, fictitious crack model, cohesive zone model, continuum damage mechanics, small crack merging mechanism, molecular deformation kinetics,*

I. Introduction

The application of the (structural impossible) strain softening postulate for fracture, is strictly against theory, and results, since long, in a tremendous spill of research efforts, without any possibility of progress. The lack of theory is also leading to models (see e.g. the German controlled CIB-W18 papers), where all viscoelastic, plastic, and structural change processes in e.g. beam type specimens at loading, (which are known from molecular deformation kinetics [1]), are regarded as one fracture process. This results in a never ending stream of publications of assumed R-curves. The non-existence of the hardening R-curve for wood is nevertheless known from relevant small- and plate specimen data, showing no kinks in the loading line, while the kinks at mode II loading of edge notched beams is shown in [2] to be due to necessary plastic stress redistribution.

Despite this assumed hardening, a softening transformation is assumed at crack extension. This softening postulate leads to impossible models, e.g. with negative spring constants, anti-normality, negative dissipation, etc., all strictly against admissibility and against the possibility to predict strength in any circumstance. The last representative of this ineffectual movement is the cohesive zone model, which is, as all the applied empirical models, based on the general error to regard the nominal stress to be the actual stress at the fracture plane.

To try to correct this convincingly in the light of exact theory, it will be shown that real strain softening does not exist, and thus is not a material property. Yield drop (wrongly called softening) is only possible in a constant strain rate test, when the rate of the unloading process is higher than the loading rate by the constant strain rate test. Yield drop ("softening") therefore is not possible in a constant loading rate test and also not in a dead load to failure test. Also when instability is involved in the dead load test, yield drop is not possible. "Strain softening" thus, is not "softening", but is elastic unloading of the actual stress of the intact, not ultimate loaded, part of the specimen, thus outside the fracture region. Apparent and real (e.g. thermal) softening are fully described by (exact) deformation kinetics [1], without the need of impossible physical properties. It will be shown, that the real, actual stress at the fractured plane never is able to show yield drop and always determines strength behavior, what involves that deformation kinetics always has to be applied.

II. Discussion of the Fictitious crack models

The cohesive zone model is mostly qualified as a (Hillerborg type) fictitious crack model, thus is based on a fictive crack length extension, which is loaded by a cohesive flow stress, over such a length that the singularity due to this cohesive flow stress neutralizes the singularity due to the field stress at the extended crack tip. The extended crack length is however not fictitious, but real, because only then, there is a real singularity possible at a real extended crack tip, which can be neutralized. The singularity is not neutralized at the existing crack tip when this crack extension is not real. Calculated thus is the strength of an extended crack length in a stress field, loaded also by a physical and structural not possible internal opposite applied, liquid-like, viscous soften-

ing stress field near the crack tips. Although the aim of the fictitious crack models (Dugdale, Barenblatt, Hillerborg) initially was, to remove the infinite high stresses of the singularity approach, it later simply was assumed, that by the fictive softening boundary condition, the strength, of the real crack tip singularity, approaches zero, in stead of going to infinity.

These approximation models, with arbitrary outcomes (due to the impossible, now arbitrary chosen, softening boundary condition and wrong failure criterion), need not to be followed, because it is not necessary to choose an approximation of an approximation. Thus to choose a correction on the singularity solution of the Airy stress function. In chapter 2 of [2] the exact boundary value limit analysis approach, without singularities, is presented, leading to an exact Wu-failure criterion. The same can not be derived by the, singularity methods, which lead to an ultimate stress criterion for combined loading. Thus mode I and/or mode II failure is predicted to be determining, depending on which critical value of the two is the first reached. Thus an up to 100 % overestimate of the strength is in principle possible as follows from the exact (Wu-) equation, and the singularity method and the thereupon based fictitious crack models, thus are not exact for the mixed mode loading case.

The most near to exact, for uniaxial loading, is, (according to elastic-plastic limit analysis), the Dugdale method, and the results can be compared with the results of the exact solution. Then, the extended crack length r_p, according to the Dugdale model is:

$$r_p = \frac{\pi}{8} \cdot \left(\frac{K_{Ic}}{\sigma_f} \right)^2 = \frac{\pi^2 \sigma^2 c}{8 \sigma_f^2}, \tag{2.1}$$

where σ_f is a yield stress. This leads to a maximal crack opening displacement δ_c at the crack tip of:

$$\delta_c = \frac{8}{\pi E} \cdot \sigma_f \cdot r_p = \frac{K_{Ic}^2}{E \sigma_f} = \frac{\pi \sigma^2 c}{E \sigma_f} \tag{2.2}$$

when r_p from eq.(2.1) is substituted. This result, based on singularity equations, was necessarily based on very small values of r so that all terms (of the Airy stress function solution) containing not the factor $r^{-0.5}$ were neglected at the derivation of the solution equation. For finite values of r, and for the singularity neutralization effect by superposition of yield stresses, this is not allowed, leading to a not correct result. According to the exact theory, Chapter 2 of [2], applies, for Mode I, at the crack tip boundary r_0, at the start of flow, the condition: $r_0 = 2c\left(\sigma / \sigma_f\right)^2$, according to eq.(2.29) of [2] for the elliptic crack tip and applies approximately: $r_0 = c\sigma^2 / 2\sigma_f^2$ according to eq.(2.20) of [2] for the circular crack tip of the singularity approach, showing a difference by a factor 4, depending on neglected terms and form of the crack tip determining value of the tangential tensile stress along the crack-tip boundary. The Dugdale numerical factor: $\pi^2 / 8 = 1.23$ (based on an enlarged crack length) is between these values of 0.5 and 2, but is too far away from the elliptic value 2, which applies as highest lower bound of limit analysis (which bound is equal to the measurements, thus is the solution). Also the theoretical elastic elliptic crack opening displacement of: $\delta_c = (2\sigma c) / E$ is far above the Dugdale value. The Dugdale model thus shows a not exact, too low, thus rejectable, lower bound of the strength, which only applies for uniaxial loading.

A similar rejection applies for the Hillerborg cohesive zone model, which is based on "closing" stresses, proportional to the "softening" curve, because it wrongly is based on the nominal stress change, which is the decreasing elastic actual stress of the intact part, outside the fracture plane, and thus is not based, (as necessary for a right solution, see § 3, [1], [2], [3]), on the actual stress at the fracture plane, which is a, by stress spreading, [4], increasing, actual stress. Therefore, wrongly, a zero tangential stress is found at the location of the highest (strength determining) tangential tensile stress at the crack boundary. This error is of course opposite from right, as further discussed later, based on the exact derivation of the, "softening" called, yield drop curve.

III. Continuum damage mechanics

Continuum damage mechanics [3], is a simplified application of needed Deformation Kinetics analysis (of [1]), leading to the most elementary damage kinetics equations. Regarding fracture mechanics of [3], the analysis is based on the fractured (lost) area A of an initially undamaged section A_0, leading to the variable:

$$\psi = \frac{A_0 - A}{A_0} \tag{3.1}$$

The actual stress σ_a on the material then is (expressed, as wanted, in the nominal stress σ):

$$\sigma_a = \frac{P}{A_0 - A} = \frac{P}{A_0 \psi} = \frac{\sigma}{\psi} \tag{3.2}$$

where σ is the nominal stress and σ_a the actual tress on still undamaged (=actual) area of the section. Now:

- 1. The actual stress on the actual area evidently determines the rate of damage growth, and:
- 2. The strain increase due to damage is caused by the actual stress at the damage location.

Thus, the stress-strain behavior of the damaged material can be represented by the constitutive equation of the virgin, undamaged, material with the stress, in it, replaced by the actual stress. Thus:

$$\varepsilon = \frac{\sigma_a}{E} = \frac{1}{E} \cdot \frac{\sigma}{\psi} = \frac{\sigma}{E'} \tag{3.3}$$

with: $E' = E\psi$. A simple form of the deformation kinetics damage equation for uniaxial tension is:

$$\frac{d\psi}{dt} = -C\left(\frac{\sigma}{\psi}\right)^n \tag{3.4}$$

This is comparable with the deformation kinetics equation of [1] and § 5:

$$\frac{dN}{dt} = -CN_0 \exp\left(\frac{\sigma\lambda'}{kN}\right), \tag{3.5}$$

for a forward zero order reaction due to high stress, where the exponential equation is replaced by its power law representation in eq.(3.4). (See for that last: Section 4.4 of [2]).

To apply this, for a rod, loaded by a constant tensile stress σ_0 , the initial boundary condition of eq.(3.4), for a virgin material, is: $\psi = 1$ at $t = 0$, while at complete fracture: $\psi = 0$.

Integration of eq.(3.4) then gives for the time to failure: $t' = \left[C(n+1)\sigma_0^n\right]^{-1}$.

For stepwise loading then follows:

$$\sum_{k=1}^{s} \frac{\Delta t_k}{t'_k} = 1; \quad t'_k = \left[C(n+1)\sigma_k^n\right]^{-1} \text{ with: } \Delta t_k = t_k - t_{k-1}, \qquad \text{k} = 1,2,\ldots..\text{s.} \tag{3.6}$$

which is Miner's rule, or the principle of linear summation, which evidently also applies for wood and timber. Important conclusions now are:

1. It is necessary to apply of the actual stress in damage equations, for right results, as is applied in [3], [2] and [1], for all existing solutions, which all are empirically verified by tests, and:
2. Limit analysis deformation kinetics [1] has to be applied, (e.g. in continuum mechanics), for exact solutions. This is discussed and applied in next sections.

IV. Softening-like behavior and fracture energy

4.1 Introduction

The derivation of "softening"- called yield drop behavior of the Griffith stress, is discussed in [2], chapter 3 and it is shown that the area under this load-displacement yield drop curve, divided by the crack area, is not the fracture energy, but the total external work on the specimen. The fracture energy is half this value and is equal to the decreasing critical strain energy release rate along the yield drop curve. For wood this factor ½ is correctly is applied for mode II. For mode I this is not the case and a two times too high value is applied. According to the, for wood applied, Hillerborg, fictitious crack model, is the fracture energy related to the newly formed fractured area, what is not a right definition because the energy then is by definition different for different initial crack lengths and thus is undetermined. Necessary is to use the Griffith definition, which includes the energy of formation of the initial crack for the total energy of full crack extension over the whole width of the specimen.

Inconsistent, with the choice to relate the fracture energy to the actual newly formed fractured area, the fictitious crack model regards the nominal stress, (which is the actual elastic stress of the intact part of the specimen) to be the actual strength stress at de fracture plane. As consequence, the (by stress spreading increasing) strength, decreases strongly by definition, proportional to the yield drop curve at crack extension and approaches zero strength at the end what is against physics and against equilibrium conditions. Further, the success of the, deformation independent, Griffith theory, (and equilibrium method of limit analysis of [2]), with its constant apparent surface energy and constant energy release rate, is ignored, but should be explained by any new theory. It therefore also is necessary to discuss the real strain energy release rate at the top of the yield drop curve, which causes the start of macro-crack extension, but is shown to be determined by a critical small-crack density [2]. It further appears that proceeded small-crack extension also determines the "softening" curve and post fracture behavior, as discussed in the following.

4.2. Mode I, hardening and "softening"-like behavior

"Softening"- like yield drop only exists for the nominal stress and not for the actual fracture stress. The Griffith stress, eq.(4.8), is a nominal stress, acting on the section $b \cdot t$ of Fig. 4.1. This stress, therefore is in reality the actual stress of the intact, not fractured, part of this specimen, which shows "softening"- like yield drop, following the Griffith locus, what thus is not strain softening (at failure) but is unloading of intact undamaged material. The actual stress at the fractured section shows hardening and quasi hardening by stress spreading and thus no softening as will be derived below. The same applies for the necked actual cross section area of steel and for reduced area of other materials. Clearly the term strain softening has to be replaced by (dynamic) elastic unloading (when the unloading process is faster than the loading rate by the constant strain rate test).

As most materials, wood shows near failure a plastic and apparent plastic (deformation independent) behavior. Plasticity causes the apparent surface energy to be much higher than the real surface energy and when the test rig is stiff enough, the top of the loading curve is shown to be blunted enough to make any stress redistribution possible and the behavior can be approximated by equivalent elastic- full plastic behavior. Therefore limit analysis applies and linear elastic fracture mechanics can be applied, up to the ultimate stress at the elastic-plastic boundary around the crack tip. The dissipation by micro cracking, plastic deformation, and friction, within this boundary, called fracture process zone, then is regarded as part the fracture energy for macro crack extension. When a specimen is loaded until "flow", before the start of yield drop, and is then unloaded and reloaded, the behavior has really become elastic-full plastic, and the real stress differs an internal equilibrium system from the linear elastic loading stresses. According to the limit theorems, initial stresses or deformations have no effect on the plastic limit collapse load, provided the geometry is essentially unaltered and thus the calculation is based on initial dimensions. Therefore also, as method of practice and of the Building Codes, calculations can be based on a reduced E- modulus up to the ultimate state and therefore also the linear elastic derivation of the elastic unloading curve of the fractured specimen, is possible, based on the compliance method, as is followed below. It also should be realized that, for wood, confined plasticity, as e.g. occurs at ultimate bending compression, can be replaced by the equivalent linear elastic bending strength. Thus a linear elastic calculation up to the crack boundary is possible and the term: "linear elastic fracture mechanics" then is in fact a pleonasm.

In Fig. 4.1, a mode I, center notched test specimen is given with a length "l", a width "b" and thickness "t", loaded by a stress σ showing a displacement increase δ of the loaded boundary due to a small crack extension. The work done by the constant external stress σ on this specimen, during this crack extension is equal to:

$$\sigma \cdot b \cdot t \cdot \delta = 2W = 2\left(\sigma \cdot b \cdot t \cdot \delta / 2\right) \tag{4.1}$$

This is twice the increase of the strain energy W of the specimen. Thus the other half of the external work, equal to the amount W, is the fracture energy, used for crack extension. Thus the fracture energy is equal to half the applied external energy, which is equal to the strain energy increase W. This follows, for the total crack length, from the difference of the strain energy of a body containing the crack and of the same body, without a crack:

$$\frac{\sigma^2}{2E_{eff}} b l t - \frac{\sigma^2}{2E} b l t = W \tag{4.2}$$

The fracture energy is also equal to the strain energy decrease at fixed grips conditions when $\delta = 0$:

$$W = t\sigma \int_{-c}^{+c} v\,da = \pi \sigma^2 c^2 t / E \tag{4.3}$$

where the last two terms give the strain energy to open (or to close) the sufficient small, flat, elliptical crack of length $2c$ and where "v" is the virtual displacement of the crack surface in the direction of σ.
From eq.(4.2) and eq.(4.3) follows that:

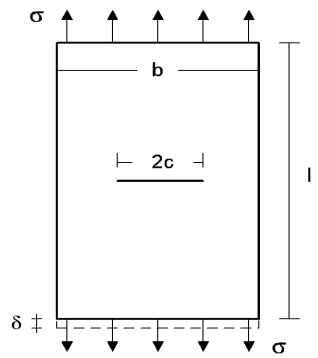

Figure 4.1 - Specimen b x l and thickness t, containing a flat crack of $2c$

$$\frac{\sigma^2}{2E_{eff}} blt - \frac{\sigma^2}{2E} blt = \pi\sigma^2 c^2 t / E \tag{4.4}$$

Thus the effective Young's modulus of the specimen of Fig.4.1, containing a crack of 2*c*, is:

$$E_{eff} = \frac{E}{1 + 2\pi c^2 / bl} \tag{4.5}$$

The equilibrium condition of the critical crack length is:

$$\frac{\partial}{\partial c}(W - G_c 2ct) = 0 \tag{4.6}$$

where G_c is the fracture energy for the formation of the crack surface per unit crack area.

With *W* of eq.(4.2) or of eq.(4.3), eq.(4.6) becomes:

$$\frac{\partial}{\partial c}\left[\frac{\pi\sigma^2 c^2 t}{E} - G_c 2ct\right] = 0, \quad \text{or:} \quad \frac{\partial}{\partial c}\left[\frac{\sigma^2 blt}{2E}\left(1 + \frac{2\pi c^2}{bl}\right) - \frac{\sigma^2 blt}{2E} - G_c 2ct\right] = 0 \tag{4.7}$$

giving both the nominal Griffith strength:

$$\sigma_g = \sqrt{\frac{G_c E}{\pi c}} \tag{4.8}$$

This stress is the actual stress P / bt outside the fractured section and is a nominal stress for the fractured section, related to the width *b* of the specimen of Fig. 4.1. The real, actual, mean stress in this weakest actual cross section (ligament) with width: $b - 2c$, where fracture occurs, is:

$$\sigma_a = \sqrt{\frac{G_c E}{\pi c}} \cdot \frac{b}{b - 2c} = \sqrt{\frac{G_c E}{\pi b}} \cdot \frac{1}{(\sqrt{c / b}) \cdot (1 - 2c / b)} \tag{4.9}$$

Because this stress is determining for newly formed crack area, it is applied by the fictitious crack models for a local fracture energy estimation. It is however not noticed that this use of the actual stress leads to "hardening", in stead of "softening", according to:

$$\frac{\partial \sigma_a}{\partial(\sqrt{c / b})} = \sqrt{\frac{G_c E}{\pi b}} \cdot \frac{6c / b - 1}{(c / b) \cdot (1 - 2c / b)^2} > 0 \tag{4.10}$$

This occurs when *c/b* > 1/6, what always is the case for actual critical crack lengths. The real actual stress σ_a increases with the increase of the crack length even up to infinity when 2*c* approaches *b* and hardening behavior characterizes the critical stress. However, there is a maximal value for this clear wood fracture as discussed in § 6. This constant maximal value of the energy release rate for each mode is basic for the Griffith theory. Then the nominal stress follows the Griffith locus, eq.(4.12) (see Fig. 4.6), as failure condition, which also is the condition of no damage acceleration, and the applied strain rate, at the end of the test is relatively slow, so that it has to be increased highly, (by one order in [5]), to shorten the delay time of the macro crack fracture process.

The stress for e.g. the minimal critical crack length of *c/b* = 1/6, is: $\sigma_c = \sqrt{G_c E / \pi c} = \sqrt{G_c E / (\pi\ b / 6}$ and the actual stress at the fracture plane is: $\sigma_{c,u} = \sqrt{G_c E / (\pi\ b / 6)(\ b / (b - b))} = 1.5\sqrt{G_c E / (\pi b / 6)}$.

Thus is 1.5 times the nominal Griffith stress. Thus, macro crack extension demands an increase of the tensile strength. The possible tensile strength increase, follows from the exact stress spreading theory of [4]. Although derived for local compression, the sign of the shear stresses may be reversed and the same spreading rules apply for tension. For *c/b* = 1/6, according to Fig. 4.1, there is a spreading of the stress on 4*c* solid material to: $b = 6c$. Thus the tensile strength is: $\sqrt{6 / 4} \cdot \sigma_m = 1.22 \cdot \sigma_m$, thus 1.22 times the uniaxial tensile strength σ_m. The nominal, fully spread, stress then is $\sqrt{4 / 6} \cdot \sigma_m = 0.82 \cdot \sigma_m$. Thus a factor 1.5 lower. High peak factors occur at long initial cracks, but there is a maximal value due to maximal possible spreading. Also the fully spread stress remains too high to explain macro crack extension at low mean stresses, where also the fracture energy is too low. Thus total fracture can not be due to single macro crack extension alone (see § 4.7). As known, a system of small cracks in the ligament, may lower the load of the adjacent intact, undamaged, part of the specimen and a high concentration of small cracks appears to be necessary to explain fracture at low nominal stresses. Because unloading is determined by the decrease of stiffness of the specimen, by crack extension, the mathematical expression of this influence has to be derived. This is discussed in the next paragraph 4.3.

4.3. The "softening"- called, yield drop curve

"Softening" (yield drop) should be described by Deformation Kinetics [1] but an alternative description of the so called "softening" behavior as a result of former crack propagation alone is possible by the Griffith theory, which can be regarded as an equilibrium method of limit design. Straining the specimen of Fig. 4.1 to the ultimate load at which the initial crack will grow, gives, according to eq.(4.5):

$$\varepsilon_g = \sigma_g / E_{eff} = \sigma_g \cdot \left(1 + 2\pi c^2 / bl\right) / E \tag{4.11}$$

Substitution of $c = G_c E / \pi \sigma_g^2$, of the ultimate state, according to eq.(4.8), gives:

$$\varepsilon_g = \sigma_g / E + 2G_c^2 E / \pi \sigma_g^3 bl \tag{4.12}$$

This is the equation of critical (unstable) equilibrium states, representing the apparent softening (= unloading) curve, due to the Griffith stress, eq.(4.8), which is the actual stress on the intact part of the specimen, outside the fracture plane. It is shown by the dynamics of crack propagation that the velocity of crack propagation is zero at the initial critical crack length and that the Griffith relation, eq.(4.8), is the condition for zero acceleration of crack extension. Thus the crack of Griffith length is in unstable equilibrium but does not propagate. The "softening"- called yield drop curve, eq.(4.12), is known as "Griffith locus" and has a vertical tangent $d\varepsilon_g / d\sigma_g = 0$, occurring at a crack length of:

$$c_c = \sqrt{bl / 6\pi}\ , \tag{4.13}$$

which is the top of the curve. Smaller cracks than c_c are unstable because of the positive slope of the locus (see eq.(4.16), because crack recovery is not possible). These small cracks, (if any, near the macro-crack tip) extend during the loading stage, by the high peak stresses at the notch of the test specimen, to a stable length and only higher crack lengths than c_c are to be expected at the highest stress before yield drop, giving the stress-strain curve of Fig. 4.2 with σ_c of eq.(4.15) as top value. For a distribution of small cracks, in a repeating pattern, *b* and *l* in eq.(4.13) are the St. Venant crack distances and the critical crack distance for extension is about 2.2 times the crack length. Because, when $b \approx 2.2 \cdot (2c_c)$ and: $l \approx 2.2 \cdot (2c_c)$, then: $bl \approx 19 \cdot c_c^2 \approx 6\pi\ c_c^2$ according to eq.(4.13). This also applies for extended small cracks after merging because the stress flow around the crack needs the St Venant's distance below the crack to be on full strength and to be able to extend the there present small cracks further. Thus the critical crack density, for the start of yield drop, is reached, when the small crack distance is about the crack length. This critical distance also is predicted by Deformation Kinetics, discussed in § 5, and is used in § 4.6 to explain yield drop by small-crack propagation in the fracture plane (at the ligament).

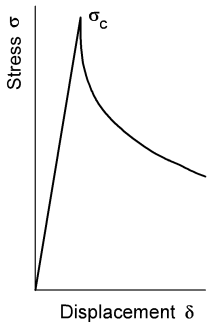

Figure 4.2 – "Softening" curve according to eq.(4.12) for the specimen of Fig. 4.1 or 4.5.

According to eq.(4.13), the yield drop line, eq.(4.12), now can be given as:

$$\varepsilon_g = \frac{\sigma_g}{E}\left(1 + \frac{\sigma_c^4}{3\sigma_g^4}\right), \tag{4.14}$$

where: $\sigma_c = \sqrt{E G_c / \pi c_c}$ (4.15)

is the ultimate load with c_c according to eq.(4.13). The negative slope of the Griffith locus is:

$$\frac{\partial \sigma_g}{\partial \varepsilon_g} = -\frac{E}{\frac{\sigma_c^4}{\sigma_g^4} - 1} \tag{4.16}$$

Vertical yield drop occurs at $\sigma_g = \sigma_c$, and the strain then is: $\varepsilon_{gc} = (\sigma_c / E) \cdot (1 + 1/3)$ and eq.(4.14) becomes:

$$\frac{\varepsilon_g}{\varepsilon_{gc}} = 0.75 \cdot \left(\frac{\sigma_g}{\sigma_c} + \frac{\sigma_c^3}{3\sigma_g^3} \right), \tag{4.17}$$

More in general eq.(4.14) can be written, when related to a chosen stress level σ_{g1}:

$$\frac{\varepsilon_g}{\varepsilon_{g1}} = \frac{\sigma_g}{\sigma_{g1}} \cdot \frac{1 + \sigma_c^4 / 3\sigma_g^4}{1 + \sigma_c^4 / 3\sigma_{g1}^4} \tag{4.18}$$

To control whether σ_c changes, eq.(4.18) can be written like:

$$\frac{\sigma_c}{\sigma_{g1}} = \left(\frac{3 \cdot (\sigma_g / \sigma_{g1})^3 \cdot \left((\varepsilon_g / \varepsilon_{g1}) - (\sigma_g / \sigma_{g1}) \right)}{1 - (\varepsilon_g / \varepsilon_{g1}) \cdot (\sigma_g / \sigma_{g1})^3} \right)^{0.25} \tag{4.19}$$

with the measured values at the right hand side of the equation. When the occurring "softening" curve starts to differ from the Griffith locus, σ_c decreases, causing a steeper decline of the curve, due to additional small crack and clear wood failure of the fracture plane. This failure by a small-crack merging mechanism is discussed in § 4.6. To measure the fracture energy as area under the softening curve, the displacement of the loading jack due

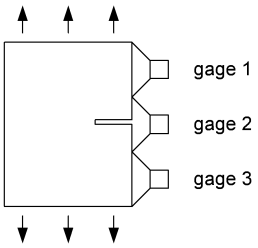

Figure 4.3. Measuring nonsense data at gage 2

to the mean deformation of the specimen has to be known. This can not be obtained by measuring the gage displacement over an crack opening (see Fig. 4.3) because it is not known what then is measured and this local unloading, around the open crack, is mainly proportional to the crack length itself, and is not simply related to the constant ultimate stress state of the ligament.

4.5. Empirical confirmation

The measurements of [5] are complete by measuring the whole loading and yield drop curve and using the compact tension tests as control, being also a control by the different loading case. The graphs of [5], Fig. 4.6 and 4.7, are the result of tension tests on the specimen of Fig. 4.5. The length of the specimen was l = 3 mm, the width and thickness: $b = t$ = 20 mm and the notch length $2c$ = 2x5 = 10 mm with a notch width of 0.5 mm. In figures 4.6 and 4.7, measured stress-displacements are given together with the lines 1 and 2 according to Griffith locus: eq.(4.17). The strain ε_g follows from the displacements at the *x*-axis of the figures, divided

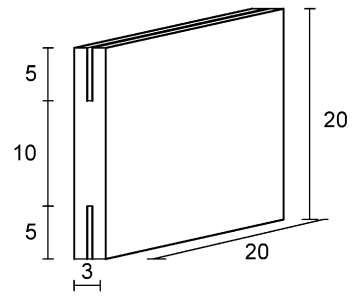

Figure 4.5 - Geometry of the specimens [5]

through 3 mm, the measuring length and length of the specimen. Because of the small length of 3 mm, not the whole width *b* of the specimen is active. Assuming a possible spreading of 1.2:1, through the thickness of 1.25 mm above and below the side notches, the working width b_{eff} is equal to the length of the fracture plane plus 2 times 1.2 x 1.25 or b_{eff} = 10 + 3 = 13 mm.

Thus the notch lengths in Fig. 4.5 should be regarded to be 1.5 mm in stead of 5 mm. The stresses in the figures 4.6 and 4.7, are related to the length of the fracture plane, thus are actual stresses and are not related to b_{eff} according to the nominal Griffith stress, wherefore the actual stresses have to be reduced by a factor: 10/13 = 0.77, as done and discussed in [2].
Macro crack extension occurs by small crack merging with the macro crack tip. Thus is due to small-crack propagation toward the macro-crack tip. The level above 4 (to 4.6) MPa is measured in 3 of the 10 specimens of the discussed series T1309/2309 of [5] and an example is given in Fig. 4.6, reaching the top of Fig. 4.2, indicating that this strength of the fracture plane according to crack-pattern A of fig. 4.8 was determining for yield drop. The other specimens of this series did show lower strength values than about 4 MPa, as applies for further unloading due to already extended small cracks.

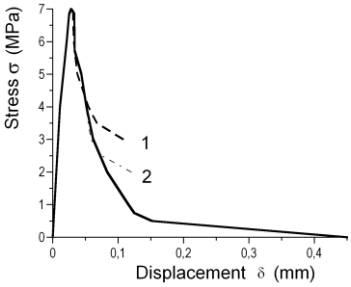

Figure 4.6 - Stress - displacement of specimen T 1409 of [5].

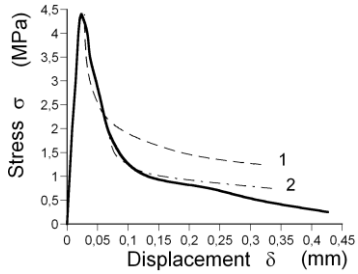

Figure 4.7 - Stress - displacement of specimen T 1509 of [5]

At § 4.3 and § 5 is shown that for the critical small crack density of eq.(4.13), the crack distance is about the crack length, as given by row A of Fig. 4.8. Line 1 of Fig. 4.6 gives the primary crack extension, eq.(4.17), by this critical crack density. Curve 1 levels off from the measurements at σ = 4 Mpa, where the next process starts, given by line 2. This thus happens when the crack length has become about 3 times the initial critical value $c_{c,0}$, according to

$$\sigma_g = \sqrt{\frac{E G_c}{\pi 3 c_{c,0}}} = 0.57 \cdot 7 = \cdot 4 \text{ MPa} \qquad (4.20)$$

This 3 times larger crack length is given by crack row B of Fig. 4.8. The top value σ_c of the first process on row A, is σ_c = 7 Mpa, for all values of σ_g between 4 and 7 Mpa. The top value of the second process B on $3c_{c,0}$ cracks, is: σ_c = 4 MPa. This process ends, where cracks of $7c_{c,0}$ lengths remain, according to row C of Fig. 4.8. Thus when:

$\sigma_g = \sqrt{\frac{E G_c}{\pi 7 c_c}} = \frac{1}{\sqrt{7}} \sqrt{\frac{E G_c}{\pi c_c}} = \frac{1}{\sqrt{7}} \cdot 7 = 0.378 \cdot 7 = 2.65$ Mpa (where line 2 of Fig. 4.6 levels off from the data)

This stress is equal to top value σ_c of the next process C, on $7c_{c,0}$ cracks, given below line 2 in Fig. 4.6. This ends at: $(1/\sqrt{15}) \cdot 7 = 0.258 \cdot 7 = 1.81$ Mpa, where the process on 15 $c_{c,0}$ starts. However, processes towards the longer cracks of 15, 31 and 63 $c_{c,0}$ are not distinct and it is probable that, due to the high actual stress, failure may occur at any point of the still intact part of the ligament.

Again, due to the spreading effect very high tensile stresses are theoretically possible, but overcritical crack lengths just show empirically too low K_{Ic} values, showing the Griffith strength and critical energy release rate to be not followed. Thus failure by post-critical crack lengths is due to ultimate uniaxial clear wood tensile stress, (or shear stress for mode II) and is not due to a critical release rate. This will be discussed further at § 4.7.

It now is shown, that the Griffith yield drop equation, combined with the crack merging model, precisely explains the data of strong specimens. The data of the less strong specimens, given by Fig. 4.7, show instability of process A, due to the steep slope near the top of Fig. 4.2. (This also explains the high variability found in [5]). Line 1 of Fig. 4.7 is the same as line 2 of Fig. 4.6, and can be chosen to level off at about 2.2 MPa, in accordance with the uniaxial strength of the still intact area of the ligament, which is half the area at 4.4 MPa, showing again that an ultimate stress criterion is determining above the nominal Griffith strength criterion for long small-cracks (thus at low nominal stress). The crack merging mechanism, clearly noticeable at strong specimens, is a chosen lower bound equilibrium system of limit analysis, which precisely follows the measured data (See § 4.6).

4.6. Crack merging mechanism

The increased unloading (yield drop), with respect to macro crack extension due to small crack extension, at the fracture plane, can be explained, using the equilibrium method, by the joining of the small cracks as follows:. In § 4.3 and § 5 it is shown, that the critical intermediate small crack distance, for crack extension, is about equal to the crack length, as given in scheme A below. In § 4.3, a crack distance of 2.2 times the crack length is found, what for simplicity of the model is rounded down here to 2, giving slightly too high stresses. For these small cracks, the critical crack length according to eq.(4.13) then is:

2c 2c 2c 2c 2c 2c 2c 2c 2c 2c 2c 2c 2c 2c . A

6c 2c 6c 2c 6c 2c 6c . B

14c 2c 14c . C

Figure 4.8. Small crack merging

$c_c = \sqrt{lb/6\pi} = \sqrt{2.2\cdot(2c_0)\cdot 2.2\cdot(2c_0)/(6\pi)} = 1.0\cdot c_0$, for the specimen with row A.

The distance *l* between the rows, above each other, is 2.2 times the crack length, being the Saint-Venant distance for building up the stress again behind a crack, to be able to form a new crack. Thus $l = b = 2.2\cdot 2c$ for row A, and $l = b = 2.2\cdot 6c$ in row B, and $l = b = 2.2\cdot 14c$ for row C. Thus when crack pairs of row A join together, a crack length of 6*c* occurs. The critical crack length thus is for row B:

$c_c = \sqrt{lb/6\pi} = \sqrt{2.2\cdot 6\cdot 2.2\cdot 6\cdot c_0^2/(6\pi)} = 0.5\sqrt{(6\cdot c_0)^2} = 0.5\cdot 6c_0 = 3c_0$.

But at the end of this process the real distances are: $6\ c_0 + 2c_0 = 8\ c_0$, and

$c_c = \sqrt{lb/6\pi} = \sqrt{8\cdot 2.2\cdot 6\cdot c_0^2/(6\pi)} = 2.4c_0$, so that the produced crack of $3\,c_0$ is overcritical and the critical process for further fractureis due to an other process. The only possibility is that small crack formation and pro pagation in the remaining intact part of the ligament becomes determining. This determining clear wood failure, which starts at half way the yield drop, is discussed in § 4.7.

For every successive process applies, that every crack merges with one neighbor by extension at one side over a distance of $1\ c_0$, leading to halving of the solid area of the ligament, and to an increase of the crack length by: $2c_{n+1} = 2\cdot 2c_n + 2c_0$, giving $2c_1 = 6c_0$ and $2c_2 = 2\cdot 2c_1 + 2c_0 = 14c_0$, as found before. The increase of the crack length is: $\Delta(2c) = 2c_{n+1} - 2c_n = 2c_n + 2c_0$. Including the initial crack length of $2\,c_0$, the increase of the total crack length is: $\Delta(2c) = 2c_{n+1} - 2c_n - 2c_0 = 2c_n$. (4.21)

More general for all merging cracks at any distance during time Δt this is:

$\Delta(c) = \beta_1\cdot c\cdot\Delta t$ (4.22)

and as the determining damage deformation kinetics equation this is (see § 5, eq.5.3):

$dc/dt = \beta_2\cdot c_0\cdot\exp(\sigma\varphi)$ (4.23)

when the initial site concentration c_0 is high, (zero-order reaction) as applies for row A of Fig. 3.

Eq.(4.23) can be written: $\ln(\dot{c}) = \ln(C) + \phi\sigma_v$, or, because $\varphi\sigma_{v0} = n$, is constant, independent of stress, due to

the time stress equivalence, [1], is:

$$\frac{\sigma_v}{\sigma_{v0}} = 1 + \frac{1}{n}\ln\left(\frac{\dot{c}}{\dot{c}_0}\right) \tag{4.24}$$

showing that the combined Griffith – crack-merging model is identical to common damage behavior. Regarding Fig. 4.8, it is clear that the overcritical longer cracks are not determining for crack extension, but that fracture always is due to the same micro crack extension in the remaining intact clear wood parts of $2c$ length. The damage process acts in all these parts at the same time. Thus, for the whole fracture process, from the beginning to full separation, applies, that micro-cracking in the intact part $(b - c)$ of the ligament is determining, and that the concentration is not determined by $c_c = \sqrt{lb / 6\pi}$, but by: $c_c' = \sqrt{c_1(b - 2c)^2 / 6\pi}$ $= c_2(b - 2c)$, (with $c_1 = 2.2^2$, is $c_2 = 0.5$).

The kinetics shows the same behavior as for clear wood, indicating that always the same small-crack propagation is determining. As shown in [1], always two coupled processes act, showing the same time-temperature and the same time-stress equivalence of both. One process, with a very high density of sites, provides the sites of the second low site density process, as follows from a very long delay time of this second macro-crack process at common load levels. (Of course there is no delay time for macro crack extension at a high loading stress level due to the time stress equivalence). The mode I notched specimen, discussed here, also shows the low concentration reaction by the strong yield drop behavior (of the nominal stress). The coupled processes occur for the crack merging processes, where the initial crack length is the reactant and the product is the newly formed crack length what also applies for macro-crack extension due to the crack merging process. The numerous small-cracks, growing towards the macro notch, provide the site for the macro crack to grow as second low concentration reaction process. This failure mechanism applies for every bond breaking process at any level.

4 7 Mode II shear tests

In [6], [7], results of mode II tests, called asymmetric four point bending (AFPB) tests, are given, applied on very long sub-critical initial crack lengths, which clearly represent an identical state of a former yield drop stage, because the measured K_{IIc} -values were a factor 3 to 4 lower than those of the control tests on standard single edge notched beam (SENB) test-specimens. By the standard fracture equation for this case, eq.(4.25), the value of τ_0 and K_{IIc} were obtained in [6], [7], by estimation of the energy release rate G_{II} by the compliance method at different crack lengths and, as control, by the finite element virtual crack closure method. The found too low value of G_c is now not the critical energy release, but simply the minimal elastic energy for crack closure of the very long crack. In the first eq.(4.7) is G_c then the mean crack closure energy per unit crack length, and the derivation in this equation, with $\partial G_c / \partial c = 0$, gives the condition of minimal mean crack closure energy per unit crack length, as minimum potential energy condition as applies for equilibrium, similar to the fracture energy in the ultimate state, giving the meaning of G_c, and of eq.(4.25), for overcritical crack lengths. Thus also in that case applies:

$$K_{IIc} = \tau_0\sqrt{\pi a_c}\cdot f(a / W) \tag{4.25}$$

This equation can be written, when clear wood shear failure is determining in this shear loaded specimen:

$$\sqrt{\pi a_c}\cdot f(a / W) = \frac{K_{IIc}}{\tau_0} = C_1 \text{ (constant)} \tag{4.26}$$

where τ_0 is the ultimate nominal stress. C_1 is only dependent on dimensions and stiffness factors of the specimen. This is different from the solution in [6], [7]. There the critical value of G_c, in $K_{IIc} = \sqrt{E G_c}$, is chosen to be at the 5 % offset from linearity. The common calculation in [6], [7], based on the assumption that the overcritical initial crack length is still the critical macro crack length, leads to strongly (factor 3 to 4) too low, not critical, not constant, values of G_c. C_1 then is dependent on a / W, and is determined by the compliance method and crack closure technique. This delivered right values of $f(a / W)$.

According to fig.12 of [7], there is no difference (by volume effect) between the data for W = 40 mm and W = 20 mm, thus mean values of both are here regarded.

Determining for small crack extension, at the presence of a long (post-critical) crack, is the still available intact area of: $(W - a)$ $c_1(W - a)$. The critical small crack density is proportional to this area according to eq.(4.13).

Thus, the critical macro-crack length, which is equivalent to the critical small crack density, is:

$$a_c = \sqrt{bl/6\pi} = \sqrt{(c_1 W(1-a/W)\cdot W(1-a/W)/6\pi)} = c_2(1-a/W)\ W \tag{4.27}$$

where: $l = W(1-a/W)$ and $b = c_1 W(1-a/W)$ as St. Venant distance. Thus, because W is constant, is:

For $a/W = 0.7$, is: $\sqrt{a_c}\cdot f(a/W) = c_6\sqrt{(1-a/W)}\ \ f(a/W) = c_6\cdot\sqrt{0.3}\cdot 1.0 = 0.55c_6$ (4.28)

For $a/W = 0.8$, is: $\sqrt{a_c}\cdot f(a/W) = c_6\sqrt{(1-a/W)}\ \ f(a/W) = c_6\cdot\sqrt{0.2}\cdot 1.2 = 0.54c_6$ (4.29)

For $a/W = 0.9$, is: $\sqrt{a_c}\cdot f(a/W) = c_6\sqrt{(1-a/W)}\ \ f(a/W) = c_6\cdot\sqrt{0.1}\cdot 1.67 = 0.53c_6$, (4.30)

giving the necessary constant value of C_1 of eq.(4.26) and providing the control of the empirical $f(a/W)$-values of [6], which are based on the initial macro-crack lengths of a/W = 0.7, 0.8 and 0.9. Eq.(4.28) to (4.30) show, that for this type of test specimen, with overcritical crack lengths, applies:

$$f(a/W) = 0.54/\sqrt{1-a/W} \tag{4.31}$$

Regarding fracture, it is to be expected, that the determining clear wood shear strength is the same for the above 3 cases. Thus: Eq.(4.25) also can be written, expressed in the ultimate actual shear stress:

$$\tau_u = \frac{K_{II}}{\sqrt{\pi a}\cdot f(a/W)}\cdot\frac{W}{W-a} = \frac{K_{II}}{\sqrt{\pi a}\cdot(1-a/W)\cdot f(a/W)} = \frac{K_{II}/\sqrt{\pi W}}{\sqrt{a/W}\cdot(1-a/W)\cdot f(a/W)} \quad \text{or:}$$

$$\tau_u\sqrt{\pi W} = \frac{K_{II}}{\sqrt{a/W}\cdot(1-a/W)\cdot f(a/W)}, \tag{4.32}$$

This is constant (because W also is constant for the 3 cases). Then:

For $a/W = 0.7$, is: $\dfrac{K_{II}}{\sqrt{a/W}\cdot(1-a/W)\cdot f(a/W)} = \dfrac{0.79}{\sqrt{0.7}\cdot 0.3\cdot 1} = 3.2$ (4.33)

For $a/W = 0.8$, is: $\dfrac{K_{II}}{\sqrt{a/W}\cdot(1-a/W)\cdot f(a/W)} = \dfrac{0.71}{\sqrt{0.8}\cdot 0.2\cdot 1.2} = 3.3$ (4.34)

For $a/W = 0.9$, is: $\dfrac{K_{II}}{\sqrt{a/W}\cdot(1-a/W)\cdot f(a/W)} = \dfrac{0.52}{\sqrt{0.9}\cdot 0.1\cdot 1.67} = 3.3$, (4.35)

giving a mean value of: $\tau_u\sqrt{\pi W} = 3.25\ \ \text{MPa}\sqrt{\text{m}}$, and with W = 40 mm, this is τ_u = 9 Mpa of the tested small clear specimen of 40x10x15 mm^3 glued in the centre of beam specimen [7]. Thus a/W = 0.8 means that the initial crack length $a = 0.8\cdot 40 = 32$ mm.

The optimal, (quasi critical) $K_{II,m}$ values of 0.79, 0.71 and 0.52 are determined in [6], [7] by the compliance method and the finite element crack closure technique as control, although these values are about a factor 2.5 to 4 below the real critical value. The in [6], [7] found $f(a/W)$-values of 1.0, 1.2 and 1.67, are agreed by eq. (4.28) to (4.30). Because, according to these equations:

$\sqrt{(1-a/W)}\ \ f(a/W) = c_7 =$ constant, is:

$$\frac{K_{II}}{\sqrt{a/W}\cdot(1-a/W)\cdot f(a/W)} = \frac{K_{II}}{\sqrt{a/W}\cdot\sqrt{(1-a/W)}\cdot c_7} = c_8 \quad \text{or:} \quad \frac{K_{II}}{\sqrt{a/W}\cdot\sqrt{(1-a/W)}} = c_9\ .$$ Thus:

For $a/W = 0.7$, is: $\dfrac{K_{II}}{\sqrt{a/W}\cdot\sqrt{(1-a/W)}} = \dfrac{0.79}{\sqrt{0.7}\cdot\sqrt{0.3}} = 1.72$ (4.36)

For $a/W = 0.8$, is: $\dfrac{K_{II}}{\sqrt{a/W}\cdot\sqrt{(1-a/W)}} = \dfrac{0.71}{\sqrt{0.8}\cdot\sqrt{0.2}} = 1.77$ (4.37)

For $a/W = 0.9$, is: $\dfrac{K_{II}}{\sqrt{a/W}\cdot\sqrt{(1-a/W)}} = \dfrac{0.52}{\sqrt{0.9}\cdot\sqrt{0.1}} = 1.73$ (4.38)

and for these specimens thus is:

$$K_{II,m} = 1.74\cdot\sqrt{a/W}\cdot\sqrt{1-a/W}\quad \text{MPa}\sqrt{\text{m}} \tag{4.39}$$

which is not based on a critical fracture energy, but on an ultimate, actual, clear wood, shear strength. It thus is confirmed by the data of [6], [7], that the actual mean shear strength of the intact part of the fracture plane is determining and not the, on the macro crack length based, apparent critical K_{II} - value, which is not

constant and too low for macro-crack extension. Macro crack extension is thus due to small crack merging and extension towards the macro-crack tip. There is no principal difference between mode I and mode II fracture, because failure for any stress combination, is due to reaching the ultimate, uniaxial, tensile strength at the crack-boundary near the crack tip [2]. Virtual, oblique, crack extension in the isotropic wood matrix applies for shear and all combined mode I – II failure cases as lower bound solution, which is an exact solution, being equal to the empirical Wu-fracture criterion [2], and thus is the real solution.

4.8. Mode I fracture at overcritical crack lengths

The same equations, as given in § 4 7 for mode II shear tests, apply for mode I tensile behavior for the successive increasing crack lengths by crack merging during yield drop. Thus similar to eq.(4.28) to (4.30) is**:**

For $2a/W = 3/4 = 0.75$, is: $\sqrt{a_c} \cdot f(a/W) = c_6\sqrt{(1-2a/W)}\ f(a/W) = c_6 \cdot 0.5 \cdot 1.51 = 0.75 \cdot c_6$ (4.40)

For $2a/W = 7/8 = 0.875$, is: $\sqrt{a_c} \cdot f(a/W) = c_6\sqrt{(1-2a/W)}\ f(a/W) = c_6 \cdot 0.354 \cdot 2.07 = 0.73 \cdot c_6$ (4.41)

For $2a/W = 15/16 = 0.938$, is: $\sqrt{a_c} \cdot f(a/W) = c_6\sqrt{(1-2a/W)}\ f(a/W) = c_6 \cdot 0.25 \cdot 2.87 = 0.72 \cdot c_6$ (4.42)

where, (see[8]): $f(a/W) = 1/\sqrt{1-(2a/W)^2}$ (4.43)

In [8], the exact derivation, as boundary value problem, of $f(a/W)$ according to eq.(4.43) is given, which does apply for critical crack lengths, while eq.(4.40) to (4.42) show that the relation: $f(a/W) = 0.74/\sqrt{(1-2a/W)}$ applies for overcritical crack lengths. This also applies for overcritical crack lengths of mode II, according to eq.(4.31).

It now can be concluded that the common calculation, where the overcritical crack length is treated as the critical crack length leads to too low, not constant, apparent energy release rates, which represent the minimum energy of crack closure. The same equation with the same values of the apparent release rates and the same values of $f(a/W)$ is found by fracture and clear wood failure of the intact part of the ligament, showing this process to be determining for fracture at lower stresses. Not the critical energy release rate is determining but the maximal stress, that has to follow the Wu-equation in stresses, of in stress intensity factors for zero open crack lengths according to § 6.

V. Deformation kinetics of fracture

The basic equations for fracture according to the limit analysis equilibrium theory of molecular deformation kinetics are given in § 4.4 of [1]. The basic concept of this, fundamental theory is to regard plastic flow as a matter of molecular bond breaking and bond reformation in a shifted position, what is the same as to state that flow is the result of a chemical reaction like isomerization. Thus not the composition changes, but only the bond structure of the molecules. Damage occurs when not all broken side bonds reform, providing the sites for a damage process.

The general theory, developed in [1], is based on the limit analysis equilibrium method and is, as such, an exact approach, which is able to predict all aspects of time dependent behavior of materials by the same constitutive equation, because the mathematical derivation of this general theory is solely based on the reaction equations of the bond-breaking and bond- reformation processes at the deformation sites due to the local stresses in the elastic material around these sites. The form of the parameters in the rate equations, are according to the general equilibrium requirements of thermodynamics. By expressing the concentration and work terms of the rate equation in the number and dimensions of the flow units, the expressions for the strain rate, fracture, flow, hardening and delay time are directly derived without any assumptions. To obtain simplifications, series expansion of the potential energy curve is applied, leading to the generalized flow theory, thus to a proof of this general flow model, and showing the hypotheses of this generalized theory, to be consequences of the series expansion. This theory thus applies generally, also for structural changes, giving an explanation of the existing phenomenological models and laws of fracture.

The rate equation for fracture then can be given, for high stress, as applies for fracture, by:

$$-\frac{d\rho}{dt} = \frac{2\rho}{t_r}\sinh\left(\frac{W}{kT}\right) \approx \frac{\rho}{t_r}\exp\left(\frac{W}{kT}\right) \tag{5.1}$$

where the concentration of activated units per unit volume ρ can be written: $\rho = N\lambda A/\lambda_1$ .with: N flow units per unit area of a cross section, each at a distance λ_1 behind each other, with λ as jump distance and A as area of the flow unit. The work of a flow unit W, with area A moving over a barrier, over a distance λ is: $W = fA\lambda = \sigma\lambda/N$. Because of equilibrium, per unit area, of the external load $\sigma \cdot 1 \cdot 1$ with the force on the N

flow units: NfA. Thus $\sigma = NfA$ and eq.(5.1) becomes, expressed in the nominal, macro, engineering stress σ, which is the part of the total external stress, that acts on *N*, to be found from tests with different loading paths:

$$-\frac{d}{dt}\left(\frac{N\lambda}{\lambda_1}\right)=\frac{N\lambda}{\lambda_1 t_r}\exp\left(\frac{\sigma\lambda}{NkT}\right), \tag{5.2}$$

In this equation is t_r the relaxation time. The value of *A* can be regarded constant because any change is compensated by an corrected value of f and a corrected value of λ to obtain a correct load on the flow unit and its correct volume. Eq.(5.2) can be written, with $N' = N/\lambda_1$ (the number of flow units per unit volume): $-d\left(N'\lambda\right)/dt = \left(N'\lambda/t_r\right)\exp\left(\sigma\lambda/NkT\right)$, or:

$$\frac{d}{dt}\left(\frac{\lambda}{N'}\right)=\frac{\lambda}{N' t_r}\exp\left(\frac{\sigma\lambda}{NkT}\right) \tag{5.3}$$

For this zero order reaction in wood, when the very high initial reactant concentration does not change much, the solution is:

$$\frac{\lambda}{N'}=\frac{\lambda t_f}{N_0' t_r}\exp\left(\frac{\sigma\lambda}{N_0 kT}\right)+\frac{\lambda}{N_0'}, \text{ or:}$$

$$\left(\frac{\lambda}{N'}-\frac{\lambda}{N_0'}\right)\cdot\frac{N_0'}{\lambda}=\frac{t_f}{t_r}=\frac{t_f}{t_0}\cdot\frac{kT}{\upsilon h}\exp\left(-\frac{E}{kT}+\frac{\sigma\lambda}{N_0 kT}\right)=\frac{t_f}{t_0}\cdot\exp\left(-\frac{E}{kT}+\frac{\sigma\lambda}{N_0 kT}\right) \quad \text{or} \quad (\text{with } \frac{kT}{h\nu}=1):$$

$$\frac{E}{kT}-\frac{\sigma\lambda}{N_0 kT}=\ln\left(\frac{t_f}{t_0}\right)-\ln\left(\frac{N_0'}{N_f'}-1\right)=\ln\left(\frac{t_f}{t_0}\right), \tag{5.4}$$

This last, according to Fig. 5, which applies for structural materials. Thus $N_f' = 0.5\cdot N_0'$ as also experimentally found for fracture, i.e. the crack length is about the crack distance, or the intact area has reduced to 0.5 times the initial area when macro-crack propagation starts due to small crack merging behavior, which explains the measured mode I and mode II final nominal yield drop behavior of fracture.

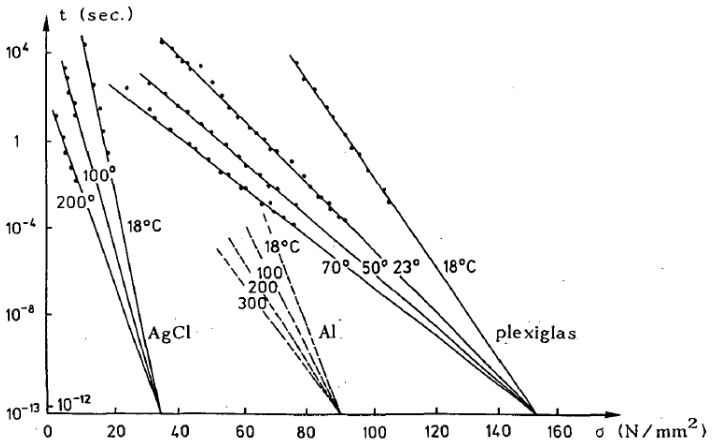

Figure 5. Stress and temperature dependence of the lifetime for structural materials [1]

VI. Small crack limit strength behavior

The interpretation of Fig. 6 in literature is to regard the inclined line to represent LEFM theory, the horizontal line to be the strength theory and the curved, connecting line to follow nonlinear fracture theory. However, there is no difference between nonlinear and linear elastic (LEFM) fracture mechanics. For both the linear elastic - full plastic approach of limit design applies. The full-plastic zone of the elastic-full plastic approach exists, as failure criterion, by a single curve in stress space as shown in Fig. 6. In this figure of [9], is d/d_0, the ratio of specimen size to the fracture process zone size. But, because the line is the result of volume effect tests, the initial crack length is proportional to the test-specimen length. Thus, d/d_0 also can be regarded to be the ratio initial open crack length to the process zone size (times a factor). Then, for small values of *d*, this d/d_0 ratio

also may represent the critical small crack density in a macro specimen (d also is crack interspace). The curved line of Fig. 6, follows the equation:

$$\ln \sigma = \ln \sigma_0 - 0.5 \ln (1 + d / d_0) \tag{6.1}$$

This can be written:

$$\ln \left| \frac{\sigma}{\sigma_0} \right| = \ln \left| \frac{d_0 + d}{d_0} \right|^{-0.5} = \ln \left| \frac{d_0}{d_0 + d} \right|^{0.5} \tag{6.2}$$

or: $\sigma \sqrt{d_0 + d} = \sigma_0 \sqrt{d_0} = K_c / \sqrt{\pi}$, (6.3)

This confirms that the curve represents the stress intensity as ultimate state with K_c as critical stress intensity factor as should be for values of d / d_0 >>1. For these higher values the curved line approaches the drawn straight tangent line $\ln \sigma = \ln \sigma_0 - 0.5 \cdot \ln (1 + d / d_0) \approx \ln \sigma_0 - 0.5 \ln (d / d_0)$ with the necessary slope of the curve $\frac{\partial \ln(\sigma / \sigma_0)}{\partial \ln(d / d_0)} \approx -0.5$ as limit. The real slope however is:

$$\frac{\partial \ln \sigma}{\partial \ln(d / d_0)} = \frac{\partial \ln(\sigma / \sigma_0)}{(d_0 / d)\partial(d / d_0)} = \frac{d}{d_0} \frac{\partial \left(\ln (1 + d / d_0)^{-0.5} \right)}{\partial (d / d_0)} = \frac{d}{d_0} \cdot \frac{-0.5}{1 + d / d_0} = \frac{-0.5}{1 + d_0 / d} \tag{6.4}$$

This slope is: – 0.5 for $d >> d_0$ and this slope is zero when $d = 0$. This shows that for the whole curve LEFM applies and it is an indication that, at zero crack dimensions, thus for: d = 0, the clear wood strength theory still follows LEFM, because it applies also for the constant initial length d_0. After first yield drop, to half way unloading, the strength theory applies for further crack extension. Similar to steel, where yield drop follows after dislocation multiplication and breakaway, applies for wood the fracture zone d_0 formation, and small crack propagation. The Wu-equation then applies in stresses [2] in stead of in stress intensities.

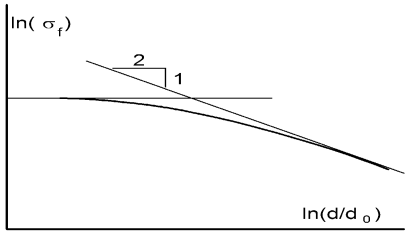

Fig. 6. From [9]. Limit LEFM behavior as correction of the interpretation of [9].

VII. Application of the singularity J-integral approach

Outer the standard methods for estimation of the energy release rate, the application of the *J*-integral (Rice integral) and *M-θ*-integral are becoming more and more a must for the singularity approaches for wood. However, the finite element applications appear to lead to quite different outcomes by different authors, showing the application to be not exact, as also follows from the following remarks, found in literature. *J* (around a singularity) is the component along the crack-line of a vector integral, having a meaning for not oblique, (thus *impossible* for shear and mixed mode [2]) and (*only for mode I*) incipient self-similar growth of a crack in a (nonlinear) elastic material. In this case, *J* has the meaning of the rate of energy-release per unit of crack-extension. The path-independency of *J* can be established only, when the strain energy density (or stress working density) of the material is a single valued function of strain. In a deformation theory of plasticity, which is valid for radial monotonic loading but *precludes unloading* and which is mathematically equivalent to a nonlinear theory of elasticity, *J* still characterizes the crack-tip field and is still a path-independent integral. However, in this case, *J* does not have the meaning of an energy-release rate; it is simply the total potential-energy difference between two identical and identically (monotonically) loaded cracked bodies which differ in crack lengths by a differential amount. Further, in a flow theory of plasticity (*as applies for wood*}, even under monotonic loading, the path-independence of *J* cannot be established. Also, under arbitrary load histories which may include loading and unloading, *J* is not only not path-independent, but also does not have any physical meaning. The blunting of the top of the loading curve and formation of the fracture zone and the main amount of crack growth with crazing and small crack formation in, (and outside), the process zone, means unloading and non-proportional plastic deformation which also invalidates the deformation theory of plasticity.
Thus the *J*- integral method, of the singularity approach, does not apply to wood.

VIII. Conclusions

- "Strain softening" called, yield drop is elastic unloading of the actual elastic stress at the intact part of the specimen, outside the fracture zone (and thus is not softening, as strain induced material transformation).
- The assumption of strain softening of the fracture stress is based on the error to regard the nominal stress to be the actual, ultimate stress, at the actual area of the fracture plane. This illogic assumption is automatically rejected because it is against fundamental properties and constitutive laws of mechanics.
- Thus, "softening"- called yield drop only exists for the nominal stress and not for the actual fracture stress, which shows hardening. The Griffith stress: $\sigma_c = \sqrt{G_c E / \pi c}$ is a nominal stress, acting on the section $b \cdot t$ of Fig. 4.1. The Griffith stress therefore only has the meaning to be the actual stress, of the intact, not fractured, not ultimate, but elastic loaded, part of this specimen, which shows yield drop at crack extension, as is common, for processes with a low reactant concentration, thus, in this case, containing a single extending macro-crack.
- This yield drop unloading, necessary for equilibrium, is due to decrease of the stiffness and increase of damage at the fracture site. The real, statically admissible, actual mean stress at the fractured region shows necessarily real and apparent hardening (by the spreading effect).
- Yield drop only is possible at a constant strain rate test, thus is not possible in a constant loading rate test and also not in a dead load to failure test. Softening called yield drop, which is elastic unloading of the intact, not ultimately loaded, part of the specimen, thus is not a material property.
- It is discussed that the fictitious crack models and the cohesive zone models are too far from theory to have any meaning. By not regarding the actual real stress, at the fracture plane, also the equilibrium, compatibility, normality, yield and boundary conditions at the crack boundary are not satisfied.
- As known from Continuum damage mechanics and Deformation kinetics, it is necessary to apply the actual stress on the actual area in damage and fracture equations, for right results, as follows from the uncountable number of solutions, which are confirmed by tests. Limit analysis, based deformation kinetics [1], has to be applied, (e.g. in continuum mechanics), for exact solutions, giving the possibility to design, reliable new, never tested, structures and to account for the influence of time (duration of load), moisture content and temperature.
- Fracture of the ligament does only at the start of yield drop follows the Griffith theory and thus is total fracture not due to single macro crack propagation alone. After half way the yield drop unloading of the nominal stress, the apparent energy release rate is not high enough anymore. Further crack extension follows a small rack merging mechanism and macro crack extension is due to small-crack propagation toward the macro-crack tip. This is caused by clear wood failure following an ultimate stress failure criterion.
- According to the crack merging mechanism and according to molecular deformation kinetics there is a critical small crack density, when the crack distance is about the crack length, for the start of yield drop.
- Important is the conclusion that, after the start of yield drop, according to a critical energy release rate, further crack extension follows by an ultimate mean shear strength criterion of the intact part of the fracture plane.
- Small-crack merging explains precisely the "softening" called yield drop curve (of [5]).

References

[1] T.A.C.M. van der Put. Deformation and damage processes in wood, , Delft University Press The Netherlands, (1989). B(1989a).

[2] T.A.C.M. van der Put. A new fracture mechanics theory of wood, Nova Science Publishers NY, or more complete:: T.A.C.M. van der Put Exact and complete Fracture Mechanics of wood Theory extension and synthesis of all series C publications

[3] L.M. Kachanov. Introduction to Continuum Damage Mechanics, , Martinus Nijhoff Publishers, Dordrecht

[4] T.A.C.M. van der Put. Derivation of the bearing strength perpendicular to the grain of locally loaded timber blocks Holz Roh Werkst (2008) 66: 409–417

[5] L. Boström, Method for determination of the softening behaviour of wood etc. Thesis, Report TVBM-1012, Lund, Sweden, (1992).

[6] Yoshihara, H. (2012) Mode II critical stress intensity factor of wood measured by the asymmetric four-point bending test of single- edge-notched specimen while considering an additional crack length, Holzforschung, 66, pp 989-992.

[7] Yoshihara H. (2008) Mode II fracture mechanics properties of wood measured by the asymmetric four-point bending test using a single-edge-notched specimen, Eng. Frac. Mech. 75 pp.4727-4739.

[8] T.A.C.M. van der Put. Exact Derivation of the Geometric Correction Factor of the Center Notched Test Specimen, Based On Small Cracks Merging As Explanation of Softening , Int J Comput Eng Res (IJCER) Vol. 04, Issue 7, July 2014.

[9] I. Smith, E. Landis, M. Gong, Fracture and Fatigue in Wood, J. Wiley & Sns.